THERMOCHEMICAL CHARACTERIZATION AND ENVIRONMENTAL EVALUATION OF COVID-19 RELATED MEDICAL WASTE

A THESIS SUBMITTED TO
THE GRADUATE SCHOOL OF NATURAL AND APPLIED SCIENCES
OF
MIDDLE EAST TECHNICAL UNIVERSITY

BY

UMUT GÜÇLÜ

IN PARTIAL FULFILLMENT OF THE REQUIREMENTS
FOR
THE DEGREE OF MASTER OF SCIENCE
IN
MECHANICAL ENGINEERING

AUGUST 2023

Approval of the thesis:

THERMOCHEMICAL CHARACTERIZATION AND ENVIRONMENTAL EVALUATION OF COVID-19 RELATED MEDICAL WASTE

submitted by **UMUT GÜÇLÜ** in partial fulfillment of the requirements for the degree of **Master of Science** i**n Mechanical Engineering, Middle East Technical University** by,

Prof. Dr. Halil Kalıpçılar
Dean, Graduate School of **Natural and Applied Sciences** _____

Prof. Dr. M. A. Sahir Arıkan
Head of the Department, **Mechanical Engineering** _____

Assoc. Prof. Dr. Feyza Kazanç Özerinç
Supervisor, **Mechanical Engineering, METU** _____

Examining Committee Members:

Prof. Dr. Derek Baker
Mechanical Engineering Dept., METU _____

Assoc. Prof. Dr. Feyza Kazanç Özerinç
Mechanical Engineering Dept., METU _____

Prof. Dr. Almıla Güvenç Yazıcıoğlu
Mechanical Engineering Dept., METU _____

Assist. Prof. Dr. Altuğ Özçelikkale
Mechanical Engineering Dept., METU _____

Assoc. Prof. Dr. Nazlı Dönmezer
Mechanical Engineering Dept., Boğaziçi University _____

Date: 17.08.2023

I hereby declare that all information in this document has been obtained and presented in accordance with academic rules and ethical conduct. I also declare that, as required by these rules and conduct, I have fully cited and referenced all material and results that are not original to this work.

Name Last name : Umut Güçlü

Signature :

ABSTRACT

THERMOCHEMICAL CHARACTERIZATION AND ENVIRONMENTAL EVALUATION OF COVID-19 RELATED MEDICAL WASTE

Güçlü, Umut
Master of Science, Mechanical Engineering
Supervisor: Assoc. Prof. Dr. Feyza Kazanç Özerinç

August 2023, 100 pages

The COVID-19 pandemic dramatically expanded the use of Personal Protection Equipment (PPE). The most commonly used PPEs against the COVID-19 virus were masks, gloves, face shields, and protective gowns. The disposable nature of most PPE generated a waste problem soon after the pandemic started. This waste problem and the constant usage of these PPE in hospitals have made it clear that there was an urgent need to investigate the thermochemical characteristics and environmental effects of the associated medical wastes. This study investigated the pyrolysis and combustion characteristics and ash compositions of the most commonly used PPEs. In contrast to previous studies, which have focused on the characterization of these waste materials individually, the present study investigated the co-combustion of PPE, which provided a realistic analysis of the ongoing waste disposal procedures. A specific combination of the medical waste blend, consisting of face mask, medical gown, and nitrile glove, was prepared based on the actual waste compositions of the COVID-19 services of several local hospitals. Thermogravimetric analysis was conducted on both the combined waste and the individual components. The results

showed a synergistic effect during the co-combustion of polypropylene-based materials with nitrile gloves, as a decrease in polypropylene-based materials' peak and burnout temperatures. Ash compositions were investigated with SEM-EDX and ICP-OES analyses. The slagging inclination of the bottom ash was investigated with conventional methods, and the results showed that slagging risks have decreased in the co-combustion of the medical wastes.

Keywords: Medical Waste, Pyrolysis, Combustion, Slagging, Ash

ÖZ

COVİD-19 SEBEPLİ TIBBİ ATIKLARIN TERMOKİMYASAL KARAKTERİZASYONU VE ÇEVRESEL DEĞERLENDİRMESİ

Güçlü, Umut
Yüksek Lisans, Makina Mühendisliği
Tez Yöneticisi: Doç. Dr. Feyza Kazanç Özerinç

Ağustos 2023, 100 sayfa

COVID-19 pandemisi ile Kişisel Koruyucu Ekipman (KKE) kullanımını önemli ölçüde arttı. COVID-19 virüsüne karşı en sık kullanılan KKE'ler maske, eldiven, koruyucu önlük ve yüz koruyucu siperliklerdir. Bu KKE'lerin tek kullanımlık olması, pandeminin başlangıcından sonra ciddi bir atık problem oluşturmuştur. Bu atık problemi ve KKE'lerin hastanelerde düzenli kullanılmaya devam edecek olması, bahsi geçen ekipman atıklarının termokimyasal karakterizasyonu ve çevreye etkisi hakkında daha fazla araştırma yapılması gerekliliğini ortaya koymuştur. Bu çalışma maske, eldiven ve önlük gibi en sık kullanılan KKE'lerin piroliz ve yanma karakterizasyonu ile kül içeriklerini incelemiştir. Bahsedilen atık malzemelerin karakterizasyonuna odaklanmış olan önceki çalışmaların aksine, bu çalışmada gerçekte uygulanmakta olan prosedürlere uygun bir analiz amaçlı KKE'lerin birlikte yanma süreçleri incelenmiştir. Bu çalışmada çevre hastanelerdeki COVID-19 servislerinde oluşan tıbbi atıkları modellemek amaçlı bir atık karışımı çalışılmıştır. Termogravimetrik analizler hem KKE'ler hem de hazırlanan karışımlar için yapılmıştır. Elde edilen sonuçlar, polipropilen içerikli malzemelerin nitril eldiven ile yanması durumunda sinerjik etki gösterdiğini ortaya çıkartmıştır. Yanma sonucu oluşan küller SEM-EDX ve ICP-OES analizleri ile incelenmiştir. Yanma sürecinde

KKE’lerin cüruf oluşum ihtimalleri geleneksel metotlarla incelenmiş olup, sonuçlar ortak yanma sürecinde bu ihtimalin düşüşünü göstermiştir.

Anahtar Kelimeler: Tıbbi Atık, Piroliz, Yanma, Cüruf, Kül

To My Lovely Family

ACKNOWLEDGMENTS

First, I want to express my sincere gratitude to my supervisor, Assoc. Prof. Dr. Feyza Kazanç Özerinç for her guidance, support, and advice during my thesis studies, as well as her friendship and kindness.

During my studies, I had the opportunity to collaborate with several people. Among them, I wish to express my most sincere appreciation and gratitude to Dr. Anna Trubetskaya from Nord University for our collaborative studies and her mentorship during our research. I would like to thank Dr. Italo Pisano from the University of Limerick for his support and contributions to my studies, especially with ICP-OES analysis. I want to thank METU MERLAB employees for their assistance with various analyses.

I want to thank Prof. Altan Kayran from the Department of Aerospace Engineering, METU, for granting access to the Thermogravimetric Analyzer, Fourier Transform Infrared Spectroscopy, and Differential Scanning Calorimetry at Composite Materials Characterization Laboratory in the Center for Wind and Energy Research. His support allowed me to improve myself and complete my thesis.

I would like to express my sincere thanks to my lab colleagues Alican Akgül and Süleyman Şener Akın for their constant help and invaluable friendship.

Finally, I would like to thank my family, who have supported and encouraged me through my education.

TABLE OF CONTENTS

LIST OF TABLES

TABLES

LIST OF FIGURES

FIGURES

CHAPTER 1

INTRODUCTION

On the 10th of January 2019, the World Health Organization (WHO) announced that the outbreak in Wuhan, China, was caused by the novel Coronavirus [1]. This virus causes an infectious disease leading to respiratory problems and, in some cases, death. On the 11th of March 2020, WHO announced Covid-19 as a pandemic [2]. The virus is usually transmitted by close contact with infectious people through the liquid particles released from the mouth or nose during coughing, sneezing, or speaking [3]. Given the 14-day incubation period and the highly transmissible nature of the coronavirus, infected individuals can easily transmit the virus to nearby persons in their daily interactions [4]. Because of the fast-spreading nature of the virus, all countries have been affected rapidly. Until now, more than 750 million cases have been reported, including more than 6.9 million deaths [5]. According to the World Health Organization, the number of COVID-19-infected patients will continue to increase due to the ability of the virus to mutate over time [6].

Around the globe, people took different personal measures against the virus, such as using protective equipment, staying away from outside human contact, using disinfectants, etc. In addition to that, governments announced mandatory and suggested protective measures to protect the mass population against the virus. Using Personal Protective Equipment (PPE) became the most recommended protection measure. This situation generated a significant need for the widespread adoption of PPE in everyday life.

Personal Protective Equipment plays a vital role in protection against the spread of microorganisms, toxic substances, and pathogens [7]. Most of these equipment

types, particularly the ones used on a daily basis, were designed for single-use and require replacement after a few hours of usage.

Personal Protective Equipment (PPE) refers to the gear employed to reduce the risk of workplace injuries or illnesses resulting from exposure to different hazards, which can arise from various sources such as chemicals, radiation, physical forces, electricity, machinery, or biological agents. A range of PPE options exists to address specific workplace hazards, such as gloves, safety goggles, protective footwear, earplugs, hard hats, respirators, coveralls, vests, and full-body suits [8,9].

The transmission of biological agents occurs through direct or indirect contact between individuals. Considering the proximity healthcare workers maintain with patients, it is crucial for them to have access to PPE that effectively shields them from potential transmission [9].

Figure 1.1 Personal Protective Equipment: face mask, N95 mask, face shield, goggles, latex glove, nitrile glove, long nitrile glove, doctor coat, medical gown [10,11]

As outlined by the Centers for Disease Control and Prevention (CDC), the assortment of medically employed PPE within hospital settings encompasses face or surgical masks, respirators, face shields, goggles, nitrile or latex gloves, medical gowns, aprons, as well as head and shoe coverings. The most common types of PPE are shown in Figure 1.1, and their respective raw materials are shown in Table 1.1. As seen from that table, almost all PPEs are made from plastic materials, while the most common ones are polypropylene masks, polypropylene gowns, and nitrile gloves. In the context of this thesis, the focus is solely on medically utilized PPE.

Table 1.1 Raw materials of Personal Protective Equipments

Protective Equipment	Raw Material
Face Mask	Polypropylene, Polystyrene, Polyethylene, Polyester, Polyvinyl Chloride, Polyethylene Terephthalate [12] [13]
Face Shield	PLA, ABS, PET [14]
Medical Gown	Polypropylene, Polyethylene [15]
Glove	Nitrile (preferable), latex, Polychloroprene, PVC, Polyisoprene [16]
Goggles	PVC [16]

Plastic consumption related to medical equipment in healthcare facilities has experienced exponential growth due to the Covid-19 pandemic [17–19]. Biomedical waste is estimated to be 25 times the waste generated before the pandemic [17,20]. To prevent contamination and maintain the required level of hygiene, the majority of these PPE items are designed for single use and subsequently discarded after each instance of use. This disposal practice ensures that healthcare workers are equipped with clean and uncontaminated PPE for every interaction with patients, minimizing the potential spread of infectious agents and maintaining a safe environment within healthcare settings. It also leads to the creation of large volumes of medical waste.

Moreover, the daily consumption of single-use facemasks by the mass population increases the creation of non-recyclable plastic waste that has a detrimental impact on the environment. Table 1.2 gives the PPE acceptance rate by population, usage amount, and estimated medical waste generation due to PPE. The acceptance rate provided in the table represents the population's usage rate of the specified protective equipment.

The estimated daily face mask usage was over 3.3 billion, resulting in over 1.6 million tons of medical waste per day during the pandemic [21]. This consumption related to the pandemic also generated more than 584 million tons of plastic waste around the globe annually [21]. Also, in Turkey, the estimated daily face mask usage was more than 51 million piece per day, with 6.3 million tons of medical waste yearly [21].

There has been no infrastructure for the safe and environmentally friendly disposal of single-use face masks worldwide [22]. The increasing use of masks increased their manufacturing rates using high quantities of energy and water [23]. Current waste management strategies rely on thermochemical treatments such as pyrolysis and incineration of medical waste. Plastic waste is a valuable energy source considering its higher heating value (HHV), and it is an abundant material once discarded. It has an HHV of around 41-47 MJ/kg [24], much higher than coal, about 25-35 MJ/kg [25]. Recovering energy from plastic waste could reduce the reliance on fossil fuels for energy generation.

On the other hand, most PPE wastes contain polypropylene and/or polyethylene, negatively impacting human and animal safety and health [26]. During the incineration of plastic waste, greenhouse gases such as carbon dioxide (CO_2), carbon monoxide (CO), hydrogen sulfide (H_2S), nitrogen oxides (NO_x), sulfur oxides (SO_x), and other toxic substances are emitted. Also, the discharge water contains polymeric compounds, aggravating climate change and threatening human health with cancer, neurological damage, respiratory ailments, reproductive disorders, and heart diseases [18,27,28]. The presence of these pollutants highlights the requirement for strict

pollutant emission controls and effective remediation treatments before their disposal. Adaptation and further improvement of these measures can eventually minimize the environmental impact and the potential harm to human health while increasing the overall cost of the process [18].

Policymakers, industrial stakeholders, and scientists have already begun exploring alternative solutions, including reusing and reprocessing PPE by producing either consumables made from biodegradable materials or recycled plastics using thermochemical processes [29]. The effectiveness and impact of the alternative materials are not yet understood, and the research and integration of alternative materials in existing PPE manufacturing processes are ongoing [30,31].

Moreover, with thermochemical processes, biofuel or construction materials can be obtained from single-use PPE [32,33]. Resulting ash can be used in many areas of industry. Understanding the chemistry behind bottom ash utilization is complicated, as medical waste is incinerated as a blend of different medical items.

Previous studies highlighted the importance of performing fundamental laboratory scale studies to understand the interaction between individual medical items used during incineration. Despite the existence of many studies conducted at the industrial scale, more knowledge was required to optimize the performance of power plants, remain flexible in fuel selection, and improve the design of future power plants with respect to their efficiency and operational safety. Therefore, this study aims to understand the properties of both individual medical items and their blends during laboratory fixed-bed scale combustion. The composition of inorganic matter and toxicity of bottom ashes will be evaluated. The ash analysis will be performed using Scanning Electron Microscopy with Energy Dispersive X-Ray Spectroscopy (SEM-EDX) and Inductively Coupled Plasma Optical Emission Spectroscopy (ICP-OES) and traditional protocol methods to assess the reproducibility and accuracy of the inorganic matter composition. The resulting bottom ash will also be investigated for its slagging performance by its base-to-acid ratio to understand whether the process includes any risks to equipment and to find out the potential usage of the ash.

Table 1.2 Estimated total plastic waste generation due to COVID-19 by region, measured in tons [21]

Region	Population	Facemask acceptance rate by population (%)	Average Facemask/capita/day	Estimated daily facemask disposed	Estimated plastic waste generated per day (Tons)	Estimated plastic waste generated (Tons)
Africa	1,340,598,147	70	1	411,814,854	275,465	100,544,861
Asia	4,641,054,775	80	1	1,875,181,681	953,641	348,079,108
Europe	747,636,026	80	1	445,022,934	153,623	56,072,702
South America	653,952,454	75	1	380,414,703	134,373	49,046,434
North America	368,869,647	80	1	244,335,150	75,795	27,665,223
Oceania	42,677,813	75	1	21,682,379	8,769	3,200,836
Total	7,794,788,862			3,378,451,702	1,601,666	584,609,165

CHAPTER 2

LITERATURE REVIEW

This chapter provides a brief review of the literature and ongoing waste management procedures. In section 2.1, medical waste management is explained with examples from Turkey. Section 2.2 introduces polymers used as raw materials in selected medical wastes. Section 2.3 reviews PPE waste characterization methods and previous studies on that. In sections 2.4 and 2.5, thermochemical treatment methods, pyrolysis and combustion, are discussed with the existing studies in the literature. In section 2.6, co-firing in thermochemical treatments is introduced. Finally, in section 2.7, ash produced by combustion and its characterization techniques are briefly reviewed.

2.1 Medical Waste Management

In medical waste management, medical waste is collected, sterilized, and sent to medical waste facilities for further thermal treatment.

Once collected, medical waste from healthcare facilities is either sterilized on-site or transported to sterilization centers or incineration plants based on composition. Even though there are various sterilization methods available, none can sterilize medical waste enough to eliminate the potential for infection from all kinds of medical waste. These sterilization methods are typically used to sterilize hospital equipment or to reduce the risk of infection from medical waste in case there is a need for temporary storage of the medical waste before sending it to a medical waste center.

Figure 2.1 Rotary kiln incinerator scheme in Istanbul [34]

In medical waste centers, pyrolysis and incineration of medical waste are used to eliminate the infectious nature of the collected waste. By using these techniques, all the pathogens or contaminants present in medical waste are destroyed. In most cases, as well as in Turkey, incineration plants use a rotary kiln incinerator. A schematic representation of the medical waste incineration plants in Istanbul is given in Figure 2.1. These plants employ a two-stage incineration process. In the first stage, the medical waste is incinerated in a rotary kiln at a minimum temperature of 850 ^{o}C for at least one hour. In the second stage, the flue gases resulting from the initial combustion are further incinerated at 1200 ^{o}C in a second combustion chamber. Subsequently, the high-temperature gases are directed toward a steam generator, allowing for the energy recovery utilized during the incineration procedures. Following these procedures, medical waste experiences a significant reduction in volume, reaching up to 95% and in mass approximately 75% [34].

In all medical waste facilities, medical waste is handled as a whole, which means different waste items are treated together and not separated. Each waste item can affect other items during the co-combustion of different medical wastes. To understand this effect, combustion characteristic temperatures of both medical waste and its raw material should be well understood. It is important to understand this interaction to optimize incineration at the power plant because it will also have a substantial impact on the ash composition.

2.2 Polymers

This part of the thesis explains raw materials, polypropylene and nitrile, of the most commonly used PPE, face masks, medical gowns, and nitrile gloves.

2.2.1 Polypropylene

Polypropylene (PP) is a linear thermoplastic in the polyolefin family [35]. It consists of long chains of polymerized propylene structure. It was first discovered in 1954

and used widely due to its low density [36]. PP is the most commonly used polymer in nonwoven fabrics [37], including medical equipment such as face masks and medical gowns. Figure 2.2 shows the chemical structure of polypropylene with its monomer propylene.

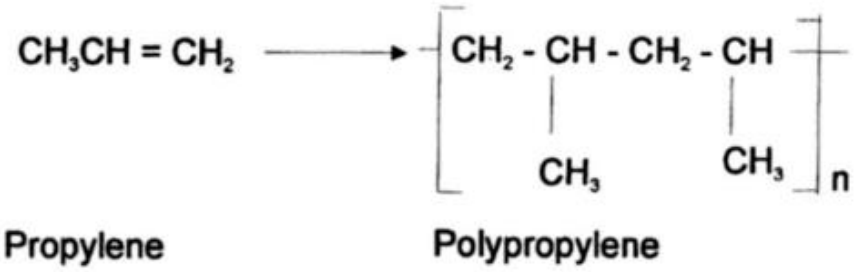

Figure 2.2 Polypropylene structure [38]

2.2.2 Nitrile

Nitrile, or acrylonitrile butadiene rubber (NBR), is the copolymer of acrylonitrile (C_2H_3CN) and butadiene $(CH_2CH)_2$ monomers [39]. Its chemical structure is given in Figure 2.3, where the right-side group, represented with the coefficient m, is the acrylonitrile monomer, and the left-side group, represented with the coefficient n, is the 1,3-butadiene group. NBR properties can be altered for desired specifications by modifying its acrylonitrile content, n/m ratio, in the chemical structure [40].

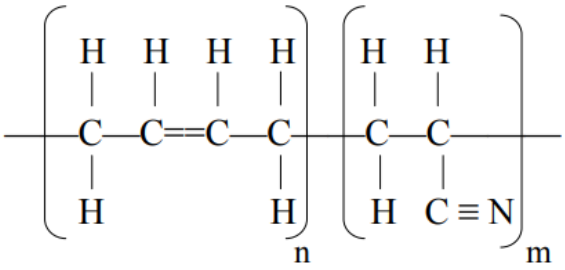

Figure 2.3 Acrylonitrile butadiene rubber (NBR) chemical structure [41]

2.3 Personal Protective Equipment Waste Characterization

This part of the thesis introduces sample characterization methods such as proximate analysis, ultimate analysis, and differential scanning calorimetry with the relevant literature studies.

2.3.1 Proximate and Ultimate Analysis

Proximate analysis is a methodology employed to determine the distribution of constituents within samples through controlled heating conditions. This analytical technique quantifies the samples' moisture, volatile matter, fixed carbon, and ash contents [42]. The procedural steps of proximate analysis can be modified to suit various sample types. However, the fundamental principle involves subjecting the sample to controlled heating within an inert atmosphere, mostly nitrogen or argon, evaporating the moisture and volatile components. After that, introducing air into the system promotes the fixed carbon's incineration, leaving only the ash content behind. Throughout each stage of the analysis, the weight of the sample is recorded to determine the quantity of each constituent.

The ultimate analysis is a quantitative methodology utilized to determine the specific carbon, hydrogen, nitrogen, and sulfur content within a sample, whether organic or inorganic, in a solid or liquid state. This analytical approach provides precise measurements of these elemental components, offering valuable insights into the composition of the analyzed matter. In the ultimate analysis, the sample undergoes combustion, converting its carbon content to CO_2, hydrogen to H_2O, nitrogen to N_2, and sulfur to SO_2. Subsequently, the combustion gases are directed from the furnace towards the detection systems, where the released gas constituents are detected. Based on the measured quantities, the determination of elemental composition is computed.

Table 2.1 summarizes proximate and ultimate analysis results of nitrile gloves, polypropylene, and face masks in the literature. As seen from Table 2.1,

polypropylene, the raw material of face masks and medical gowns, has less than 0.3% moisture content [43–49]. Most studies report polypropylene volatile matter as 99% [44,45,47–49], while two studies report more than 90% [43,46]. Some studies reported that polypropylene has less than 0.5% fixed carbon [44,45,47–49], while others reported it has up to 7% [43,46]. For ash content, most studies reported less than 0.2%[44,45,47–49], and only two studies reported to be 0.9%[46] and 2.2% [43].

Its ultimate analysis found that polypropylene has 85% carbon, 14% hydrogen, and less than 0.3% nitrogen with no sulfur content [43–50]. There are different results stated for the oxygen content of polypropylene. Some studies reported that it has no oxygen content [45,46,48,50], while in other studies, it was reported to be less than 1% [44,47], and two studies reported 2% [49] and 7% [43] oxygen content.

Face masks have less than 0.5% moisture and high volatile matter [51–60]. Two studies reported around 80% to 90% volatile matter [54,58], while other studies reported more than 90% for face masks [51–53,55–57,59,60]. Also, most studies reported less than 1% of the fixed carbon amount for face masks [52,53,55–57,60], while some reported around 2-9% [51,54,58,59]. For the ash content of the face mask, most studies reported less than 1% [51,53,56,57,59,60], but in some studies, it was reported around 3-12% [52,54,55,58].

In the ultimate analysis, face masks were reported to have around 75-85% carbon, 14% hydrogen, less than 1% nitrogen, and no sulfur content [51–62]. Most studies reported that face masks have less than 1% or no oxygen at all [51,52,56,57,59–61], while in some studies, it was reported to be up to 8% [53–55,58].

There are fewer studies on nitrile gloves compared to face masks. The proximate analysis of nitrile gloves showed less than 1% moisture content, around 90% volatile matter, and less than 6% ash [63–65]. Nitrile glove fixed carbon content was reported to be less than 0.7% in some studies [63,65], while Gerasimov et al. [64] reported

Table 2.1 Proximate and Ultimate analysis of selected materials

Moisture	Volatile Matter	Fixed Carbon	Ash Content	Reference	C	H	O	N	Reference
Proximate Analysis of Nitrile Gloves, wt%					*Ultimate Analysis of Nitrile Gloves, wt%*				
0.00	87.45	11.05	1.50	[64]	75.90	8.50	1.60	6.50	[62]
0.55	94.26	0.62	4.57	[65]	77.32	8.27	0.00	12.90	[64]
0.66	93.63	0.14	5.57	[63]	76.00	8.54	9.46	6.00	[65]
					75.99	8.26	9.41	6.34	[63]
Proximate Analysis of Polypropylene, wt%					*Ultimate Analysis of Polypropylene, wt%*				
0.28	89.90	7.64	2.18	[43]	84.31	15.30	0.00	0.31	[50]
0.00	99.50	0.50	0.00	[44]	79.60	13.05	7.36	0.04	[43]
0.00	99.58	0.42	0.00	[45]	85.56	13.85	0.59	0.00	[44]
0.00	96.48	2.63	0.89	[46]	85.38	14.62	0.00	0.00	[45]
0.00	99.88	0.00	0.12	[47]	85.03	13.99	0.00	0.09	[46]
0.00	100.00	0.00	0.00	[48]	85.85	13.78	0.37	0.00	[47]
0.00	99.92	0.04	0.04	[49]	85.48	15.42	0.00	0.00	[48]
					83.55	13.99	2.39	0.08	[49]
Proximate Analysis of Face Masks, wt%					*Ultimate Analysis of Face Masks, wt%*				
5.00	92.90	1.90	0.20	[51]	79.26	21.29	0.00	0.83	[61]
0.12	96.60	0.00	3.28	[52]	85.40	14.10	0.20	0.00	[62]
0.51	98.39	0.65	0.45	[53]	84.37	14.93	0.70	0.00	[51]
0.00	83.35	4.70	11.95	[54]	84.71	14.35	0.94	0.00	[52]
0.31	95.40	0.15	4.14	[55]	85.53	12.19	1.65	0.18	[53]
0.27	98.91	0.51	0.31	[56]	77.77	13.40	8.78	0.05	[54]
0.30	99.70	0.00	0.00	[57]	83.68	14.58	1.74	0.00	[55]
0.00	81.30	9.20	9.50	[58]	84.99	14.07	0.91	0.03	[56]
0.42	96.62	2.87	0.08	[59]	85.20	14.55	0.25	0.00	[57]
0.06	99.94	0.00	0.00	[60]	75.90	14.80	8.50	0.80	[58]
					85.65	14.43	0.00	0.00	[59]
					84.79	14.07	0.00	1.97	[60]

that same content to be around 11%. The ultimate analysis of nitrile gloves was reported as 76% carbon, 8% hydrogen, and no amount of sulfur [62–65]. For oxygen content, two studies reported less than 2% [68,70], while another two reported 9% [63,65]. For the nitrogen content of nitrile gloves, most studies reported around 6% [62,63,65], while one study reported 13% [64].

2.3.2 Differential Scanning Calorimetry

Differential Scanning Calorimetry (DSC) is a thermo-analytical technique utilized to measure the disparity in the heat absorption or release required to raise the temperature of a sample relative to a reference material. This method allows for the investigation of endothermic and exothermic transitions occurring within the sample as a function of temperature. By observing these transitions, essential information can be determined, such as the transformation temperatures associated with phenomena like glass transition (T_g), melting (T_m), and crystallization (T_c).

DSC analyses on the raw materials of selected medical wastes, polypropylene for face masks and medical gowns, and acrylonitrile butadiene rubber for nitrile gloves, have been conducted by several researchers. The literature data reveals that polypropylene's glass transition, crystallization, and melting temperatures were around -20 ^{o}C, 120 ^{o}C, and 165 ^{o}C, respectively [66–73]. Acrylonitrile butadiene rubber (NBR) is known to exhibit only glass transition, with reported values ranging from -10 ^{o}C to -30 ^{o}C, depending on the production process [74–76].

2.4 Pyrolysis

Pyrolysis can be defined as a thermochemical process where a solid or liquid carbonaceous material undergoes decomposition into smaller volatile molecules at elevated temperatures within an inert atmosphere[77,78]. It is a transformative process that yields a range of thermal degradation products, known as pyrolysis products, contributing significantly to chemical recovery [78]. Due to the absence of

oxygen, combustion does not occur during pyrolysis. Consequently, the sample undergoes thermal decomposition, releasing combustible gases [79]. The majority of the combustible gases generated during pyrolysis possess the potential to be condensed into a combustible liquid known as pyrolysis oil [77,79]. However, alongside the condensable gases, there are also permanent gases such as CO_2, CO, H_2, and light hydrocarbons [77]. Some of these permanent gases can be used for combustion, supplying the necessary heat for pyrolysis [79].

Consequently, pyrolysis yields three primary products: a liquid product called pyrolysis oil, a solid product known as char, and a gaseous product called syngas [35–37,79]. The relative proportion of these products is contingent upon several factors, including the feedstock composition and the specific process parameters employed during pyrolysis [79]. For materials that have low amounts of fixed carbon, like plastics, char formation would not be observed.

Pyrolysis has three different degradation mechanisms: random scission, side-group scission, and monomer reversion [35,37,78]. The long carbon chain's carbon-to-carbon bonds are randomly broken down in the random scission mechanism. Due to carbon bonds' uniform strength, scission is random in nature. Pyrolysis of PP is known to follow the random scission mechanism [35–37]. Contrastingly, the side-group scission mechanism involves the initial breaking of the carbon-to-side element bond rather than the carbon-to-carbon bond. Monomer reversion, also called depolymerization, consists of reversing the polymerization process and fragmenting the chain into its monomeric constituents. In this case, the carbon-to-carbon bonds break at alternating carbon atoms, leaving behind isolated monomeric units. Depending on the specific pyrolysis mode, the pyrolysis product can exist as a monomer or a series of different molecules.

The decomposition process during pyrolysis generates molecular fragments that exhibit distinct characteristics associated with the original material. These fragments can be further analyzed and identified through various techniques such as gas chromatography, mass spectrometry, or Fourier transform infrared spectroscopy

(FTIR). These analytical techniques generate a spectrum of the original material, providing valuable information for identification and comparative purposes. The spectrum is a fingerprint-like representation of the material, determining its composition and facilitating comparisons with other samples [80].

Comprehensive knowledge of the pyrolysis process is crucial to predict the reactor performance of a thermochemical process [81,82]. The most important operational parameters in pyrolysis include heating rate, pyrolysis temperature, and residence time [83,84].

According to the heating rate, pyrolysis can be classified into three categories: slow, fast, and flash pyrolysis [77,85]. In slow pyrolysis, a heating rate between 1-100 ^{o}C/min is applied, and the temperature is usually around 300-700 ^{o}C, which increases the residence time of the sample [77,84,86]. In fast pyrolysis, a higher heating rate of 10-100 ^{o}C/s is applied, and the temperature is around 550-1250 ^{o}C [77,84,86]. On the other hand, flash pyrolysis has the highest heating rate of 10^{3} - 10^{4} ^{o}C/s and temperatures around 800-1300 ^{o}C [77,84,86]. In flash pyrolysis, the residence time is very low, and it is applied when the goal is to promote gas production [77].

Also, according to temperature, pyrolysis can be classified as high or low-temperature pyrolysis. If the temperature is more than 800 ^{o}C [84], the process is called high-temperature pyrolysis; if the temperature is less than 500 ^{o}C [77], it is called low-temperature pyrolysis, and in between 500 ^{o}C and 800 ^{o}C medium-temperature pyrolysis [84].

2.4.1 Personal Protective Equipment Waste Pyrolysis

Pyrolysis has three significant characteristic temperatures: decomposition temperature (T_d), peak temperature (T_p), and end-of-decomposition temperature (T_{ed}), which can be determined from thermogravimetric-derivative thermogravimetric (TG-DTG) data [85]. The decomposition temperature is the lowest temperature at which the decomposition of a substance starts at an observable

rate and begins to break down into simpler chemical compounds [87]. It is an essential parameter for determining a sample's thermal stability and behavior. The peak temperature is defined as the temperature in the DTG profile in which the sample exhibits a significantly accelerated weight loss compared to its proximate regions. Each discrete peak in the DTG profile represents a decomposition stage of a specific ingredient present in the thermal decomposition of the sample. The term end-of-decomposition temperature is not commonly used in the literature. In the context of this thesis, it is used to signify the termination point of the decomposition process. In Figure 2.4, the identification of pyrolysis characteristic temperatures on an example DTG profile is given.

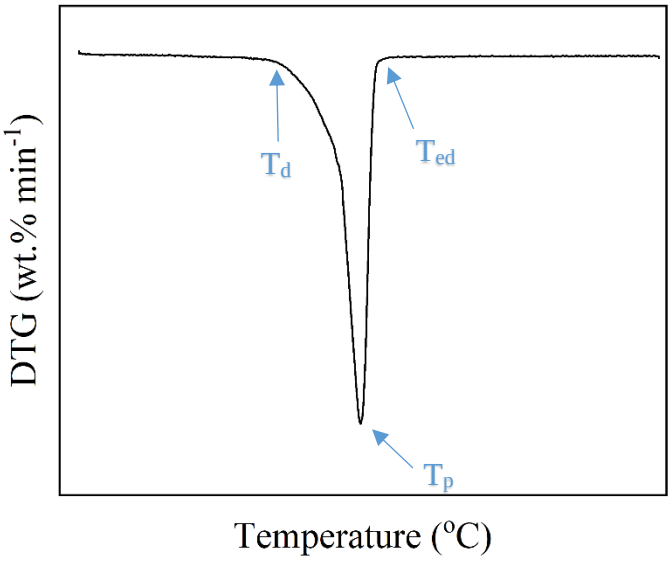

Figure 2.4 Pyrolysis characteristic temperature identification of a DTG profile

In order to understand the pyrolysis characteristic temperatures of selected medical wastes, both the raw material and waste itself were analyzed under pyrolysis conditions. The raw material of medical face masks and medical gowns is polypropylene, which has a decomposition temperature varying between 325 and

400 ℃, a peak temperature of around 460 ℃, and an end-of-decomposition temperature of around 520 ℃ during pyrolysis conditions[43–50,88–102]. Characteristic temperatures of face masks were in line with those of polypropylene, having decomposition temperature between 340 and 400 ℃, peak temperature around 460 ℃, and end-of-decomposition temperature between 470 and 490 ℃[51,52,54–62,91,103,104]. Both polypropylene and face masks have a single decomposition stage, as understood by the presence of a single peak temperature in their decomposition profiles.

The raw material of the nitrile glove is acrylonitrile butadiene rubber (NBR), which has a decomposition temperature of 350 ℃ and an end-of-decomposition temperature of 500 ℃ [105–113]. In literature, most of the studies observed a peak at 460 ℃ [105–114], indicating a single stage of decomposition, while in some studies, an additional peak around 420 ℃ was encountered[108–110,112], indicating a second decomposition stage. The decomposition and peak temperatures of nitrile gloves were in line with those of NBR, having decomposition and peak temperatures of 290 ℃ to 350 ℃ and 460 ℃, respectively, and end-of-decomposition temperature of 500 ℃ [62–65,90,115,116]. Esmizadeh et al. [121] encountered a second peak temperature of around 400 ℃ for nitrile gloves.

2.5 Combustion

Combustion is a self-sustained exothermic chemical reaction between a fuel and an oxidizer, typically oxygen for hydrocarbon fuels [117]. The combustion reaction occurs when the fuel and oxidizer mixture is within the flammability limits and is subjected to sufficient external heat to exceed the activation energy threshold [117]. It is extensively used for solid waste disposal, including plastics [35]. Up to 95% reduction in weight is achieved in plastic combustion [35].

The specific types of combustion products formed are determined by the fuel's chemical composition and the availability of carbon sites for the oxidizer to react with [117,118]. Hydrocarbon combustion reaction examples are given below:

Hydrocarbon: $4\ C_xH_y\ (g) + (4x+y)\ O_2\ (g) \rightarrow (2b)\ H_2O\ (g) + (4a)\ CO_2\ (g)$ (1)

Hydrogen: $H_2\ (g) + (½)\ O_2\ (g) \rightarrow H_2O\ (g)$ (2)

Carbon: $C\ (s) + O_2\ (g) \rightarrow CO_2\ (g)$ (3)

The given reactions are for complete combustion. Besides CO_2 and H_2O, depending on the fuel's chemical composition and combustion conditions, SO_x, NO_x, and other exhaust gases might be produced [119]. In cases when there is not enough oxygen or time to complete the reaction, incomplete combustion occurs, whereas for carbon or hydrocarbons, the output is not only CO_2 and H_2O but also CO [117,118].

Combustion reactions can be classified into two categories based on the physical state of the fuel and oxidizer involved: homogeneous and heterogeneous[117]. Homogeneous reactions occur within a single phase. The most common example of a homogeneous combustion reaction is the combustion of natural gas and air mixture, where fuel and oxidizer are in gaseous form. The second combustion chamber of a rotary kiln incinerator, where the flue gases are burned, also exhibits homogeneous combustion. On the other hand, heterogeneous reactions take place at an interface between reactants in two or more physical states, where the fuel and oxidizer mixture may not be uniformly mixed and in separate phases [117]. For example, a reaction occurs in carbon oxidation at the interface formed between the solid carbon surface and the gaseous oxidizer. The first combustion chamber of a rotary kiln incinerator exhibits heterogeneous combustion where solid medical waste reacts with oxygen.

The combustion process is a complex phenomenon in which both diffusional mass transfer and surface reaction kinetics play an important role [117]. This thesis

investigates solid waste combustion, so only solid fuel combustion is further explained below.

Solid fuel combustion occurs in four main stages [85,117]. At some point, some of these stages can happen in overlapping periods. The first combustion stage, drying, starts when the fuel gains heat from an external source. At the drying stage, gases on the solid fuel particles like water steam, methane, nitrogen, or carbon dioxide are released [120], which takes place at temperatures up to 100 – 105 ^{o}C. After the drying stage, the devolatilization stage starts at temperatures above 200 ^{o}C, depending on the fuel type. The devolatilization stage has three important physical and chemical processes: pyrolysis, volatile matter transport, and secondary reactions [117]. Secondary reactions may occur if there is enough residence time for the volatiles to react with the surrounding gas products after transforming into gaseous form.

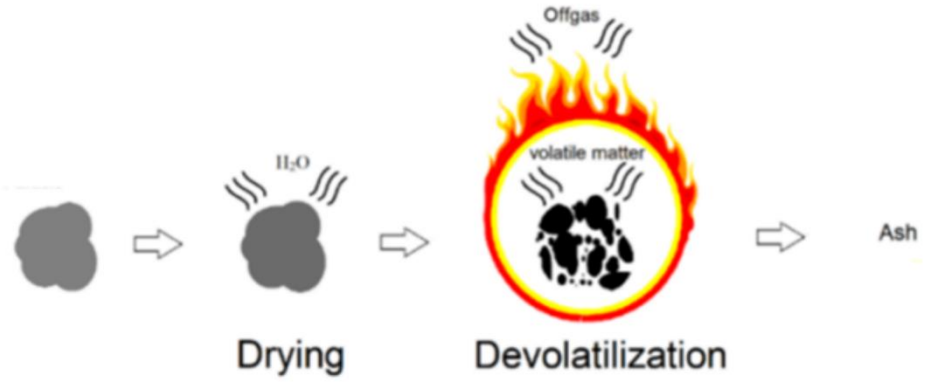

Figure 2.5 Plastic combustion process [117]

Furthermore, environmental conditions affect the volatiles released during the devolatilization stage. A higher heating rate leads to increased volatile release [121]. Once the devolatilization stage is finished, only char is left in the solid particle. In the char combustion stage, the remaining fixed carbon in the solid fuel undergoes oxidation. If the fixed carbon content is too low, like in plastics, char combustion would not be observed as a separate stage. In the end, only ash residue, a non-combustible inorganic material that the initial fuel sample had, remains.

Solid fuel combustion includes different research areas that have crucial roles in energy recovery and addressing environmental concerns, such as combustion behaviors, combustion kinetics, pollutant formation, particulate matter formation, and ash deposition [85].

For the investigation of combustion behavior, various experimental setups have been utilized. A thermogravimetric analyzer (TGA) is used in low-heating rate combustion studies. In contrast, for high heating rate combustion studies, a drop tube furnace (DTF) or entrained flow reactor (EFR) is preferred [85]. Thermogravimetric analysis for low heating rate conditions provides helpful results for determining characteristic temperatures, combustion behavior, and combustion kinetics [85].

2.5.1 Personal Protective Equipment Waste Combustion

There are three important characteristic temperatures in combustion: ignition temperature (T_i), peak temperatures (T_p), and burnout temperature (T_b), which can be determined from thermogravimetric-derivative thermogravimetric (TG-DTG) data [85]. Ignition temperature is the minimum temperature at which the sample, regardless of its physical state, spontaneously initiates and sustains combustion without the existence of an external igniting source [125,126]. The first significant change in the DTG profile that the sample starts to lose weight is identified as ignition temperature. The peak temperature is defined as the temperature in the DTG profile in which the sample exhibits a significantly accelerated weight loss compared to its proximate regions. Each discrete peak in the DTG profile represents a combustion stage of a specific ingredient present in the sample's composition. The burnout temperature is the temperature at which the fuel is at near complete combustion [127]. Identifying the burnout temperature in a sample offers essential knowledge of the dynamics of the combustion process. In Figure 2.6, the identification of combustion characteristic temperatures on an example DTG profile is given.

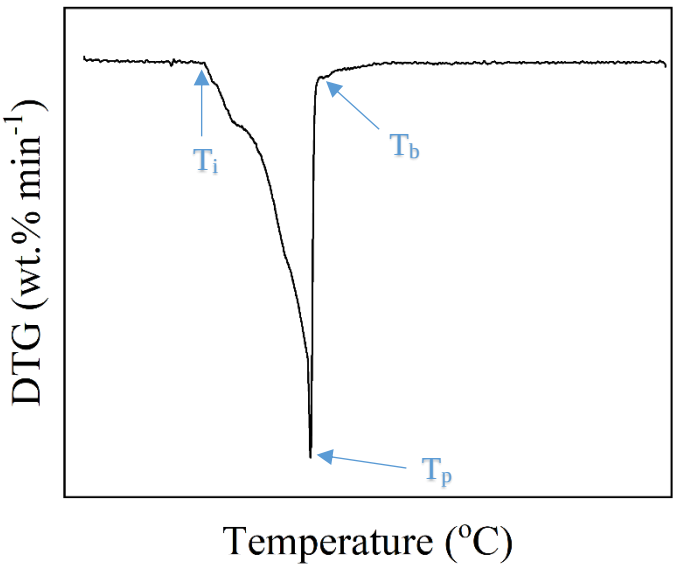

Figure 2.6 Combustion characteristic temperature identification of a DTG profile

Similar to the pyrolysis section, the raw material and waste were analyzed under combustion conditions to understand the combustion characteristic temperatures of selected medical wastes.

Polypropylene ignition, peak, and burnout temperatures were reported as 220-275 ℃, 320 ℃, and 370 ℃, respectively[93,94,97,102,128–131]. On the other hand, the burnout temperature of face masks during combustion was higher by approximately 100 ℃ compared to polypropylene, while ignition and peak temperatures were in line [51,53,103,132].

Mensah et al. [114] reported NBR ignition temperature as 375 ℃, burnout temperature as 620 ℃, and three peak temperatures at 425, 450, and 550 ℃. For nitrile glove combustion, similar results to NBR were reported as three peak temperatures at 400, 450, and 520 ℃, a lower ignition temperature at 260 ℃, and a burnout temperature at 590 ℃ [115].

Even though combustion characteristic temperatures of the selected equipment are known, their interactions with each other during co-combustion have not yet been studied. After the COVID-19 pandemic, most of the focus has shifted towards different kinds of face masks and their disposal. Considering that medical waste facilities use these equipment in the incineration process together, the co-combustion case and the equipment's interactions should also be investigated.

2.6 Co-Firing in Thermochemical Processes

Co-firing refers to the employment of more than two types of fuel simultaneously in the same chamber [133]. The most common examples of co-firing are biomass addition into coal-fired power plants or waste incineration. Co-firing in thermochemical processes can result in a synergistic effect [123,124]. This effect is seen between two or more substances that can produce a more significant result than the summation of their individual results [134], which can change the process parameters or final products in several ways, including emission reduction, process efficiency improvement, stability, fuel flexibility, and carbon capture and sequestration [123,124].

Selected fuels can interact in a way that pollutant formation, such as sulfur dioxide (SO_2), nitrogen oxides (NO_x), greenhouse gases, and particulate matter (PM), would be decreased [122]. These pollutants are very dangerous for human health and pose various environmental hazards during the operation. Mixing different types of fuels can increase the process efficiency if the added fuel acts as a catalyst for the other fuel(s). Co-firing also provides stability for the operation and offers greater flexibility in fuel choice, which is especially important for power plants. In some cases, co-firing can serve for the integration of carbon capture and storage technologies (CCS). CCS would be easier to adopt with the increased carbon dioxide (CO2) concentration in the exhaust gases.

On the other side, the ash composition left after thermochemical processes is also affected by the co-firing process [135]. Naturally, different types of fuels have different chemical compositions. In co-firing, the ash chemical composition is the combination of the adopted fuels. Also, the ashes produced by different fuels have different melting points. By changing the ash composition, the melting behavior of the ash is also affected by either an increase or a decrease in the ash melting temperature. Increasing ash melting temperature has advantages, including preventing slagging and fouling issues in thermochemical process equipment [136]. The ash composition change also affects the effectiveness of the emission control technology [137]. Specific properties of the ash, such as particle size and resistivity, can influence the performance of the controlling devices in emission control technologies.

The specific synergistic effect during co-firing can vary according to selected fuel types, specific process conditions, and the employed system design. In medical waste management, the most commonly used medical equipment is collected and treated together; therefore, they should be further investigated from this perspective to understand and optimize the employed thermochemical treatments for its gaseous emissions, effects on energy recovery, ash composition, and slagging potential.

2.7 Ash from Combustion of Solid Fuels

The combustion of solid fuel produces ash as a by-product. Ash is the non-combustible part of solid fuel, mainly composed of inorganic materials or unburned carbon, depending on operating conditions [138]. The ash comprises three main components: fly ash, boiler slag, and bottom ash [139]. Fly ash is the finest ash particles carried by the flue gases [140]. Unfiltered discharge of fly ash particles into the environment poses a significant risk to human health. Therefore, fly ash is filtered from the exhaust gases by different methods, such as electrostatic precipitators or bag filters [141]. The recovered amount of fly ash depends on the fuel's chemical composition, the operating conditions of the burners, and the boiler [139].

Slagging is the formation of molten ash or incombustible byproducts on the boiler surface, and the residue formed on the equipment is called slag. If the molten ash particles that interact with flue gases collide with the boiler wall, they rapidly cool down and solidify on the spot, leading to a significant decrease in heat transfer. Slagging poses a significant challenge to boiler efficiency and threatens the continuity of an operation [142]. Especially fuels containing high amounts of sulfur, alkali metals, or volatiles can lead to boiler hazards during energy recovery [124]. Also, another critical concern is the ash deposition on the tubes; therefore, the fouling and slagging potential of the fuels should be investigated further.

Unlike fly ash, bottom ash is characterized by coarser particle size, typically between 2 μm and 20 mm [140,143]. It consists of compact particles that cannot be transported with the flue gases due to their large and heavy particles and settle at the bottom of the furnace [139]. Bottom ash's physical properties depend on fuel type, combustion conditions, or operating temperature [140]. A significant portion of the bottom ash is utilized in the construction industry, cement manufacturing, underground mining, landfills in open mines and quarries, and fertilizer or secondary aggregates in road concentration [140,144]. Before the utilization of bottom ash in industry, it is important and helpful to investigate its chemical composition. For this purpose, various analysis methods are available, including X-Ray Fluorescence (XRF), X-Ray Diffraction (XRD), scanning electron microscopy with energy-dispersive X-Ray spectroscopy (SEM-EDX), inductively coupled plasma optical emission spectroscopy (ICP-OES), etc. In this thesis, among these methods, SEM-EDX and ICP-OES methods have been used; therefore, only these two methods are explained in the methods section.

Some studies exist on medical waste bottom ash characterization [145–147]. However, these studies often lack specifics about the collected medical waste composition and collection process. Usually, the total medical waste collected from a hospital was used directly, and their ingredients were not specified. Considering the characterization need of this medical waste and the PPE waste becoming the

increasing portion of this waste, a sample characterization was required to investigate the effects of different medical waste items on each other.

The bottom ash collected from the incineration plant is reported to be less heavy metal contaminated than the fly ash [145]. The main compounds detected in the bottom ash of an industrial-scale incinerator were Al_2O_3, SiO_2, and CaO. There were high amounts of heavy metals such as zinc (Zn), titanium (Ti), copper (Cu), cadmium (Cd), lead (Pb), chromium (Cr), nickel (Ni), and tin (Sn), which were highly leachable, therefore the most concerning for industrial uses [145,146]. However, the bottom ash composition depends strongly on the geographical location of an incineration plant with the local preferences to integrate synthetic polymers, biomaterials, or metals in PPE. Another study in Japan has also emphasized the high quantities of chlorine (Cl) in the bottom ash from blended medical waste incineration [146].

In a study performed in Wuhan, China, medical waste collected from Huoshenshan Hospital was incinerated with a mobile emergency incinerator unit, and the resulting bottom ash was investigated [147]. The findings revealed that, in the bottom ash, calcium (Ca) is the predominant element. At the same time, significant amounts of silicon (Si), magnesium (Mg), chlorine (Cl), aluminum (Al), sodium (Na), titanium (Ti), and iron (Fe) were still present in decreasing order [147].

Medical waste also contains large amounts of disposed or plastic materials, known for the high fraction of toxic metallic elements or organic compounds that might hinder bottom ash reuse [148]. In cases when incomplete combustion occurs, the bottom ash can contain persistent organic pollutants of dioxins, biphenyl, and dibenzofurans origin. Thus, it is of high importance to understand the composition and properties of bottom ash from medical waste incineration to keep a balance between health-safe, environmentally friendly, and cost-efficient applications in various industrial processes.

CHAPTER 3

METHODS AND MATERIALS

This chapter explains waste sample preparation and characterization in sections 3.1 and 3.2. Thermochemical processes used in medical waste management, pyrolysis, and combustion methodologies are presented in sections 3.3, 3.4, and 3.5. Section 3.6 explains the analysis methods used to characterize ash obtained from combustion. Finally, in section 3.7, uncertainty analysis is provided.

3.1 Sample Preparation from Personal Protective Equipment Waste

In hospitals' Covid services, doctors and nurses regularly use Personal Protective Equipment (PPE). This study analyzed the mask, glove, and gown since these were the most used PPEs. Samples were supplied from familiar brands, noting that each brand may have minor differences, mainly in mask ropes, but the main compositions were similar. Mask and gown samples were made of polypropylene, and gloves were made of nitrile. Photography of the samples is presented in Figure 3.1.

Mask samples were supplied from a common brand located in Turkey. Samples have three layers, a rope, and a nose adjustment part. All the layers are made of polypropylene, and the rope is made of cotton. The nose adjustment part was removed in the analysis. The mask layers have the same weight as each other, corresponding to 30% of the overall mask weight each, while the rope weight is only 10%. The gown is made of polypropylene non-woven fabric, and a sample was taken from a hospital for this study. Gloves were made of nitrile, and samples were supplied from a company located in Germany that provides laboratory equipment in Turkey.

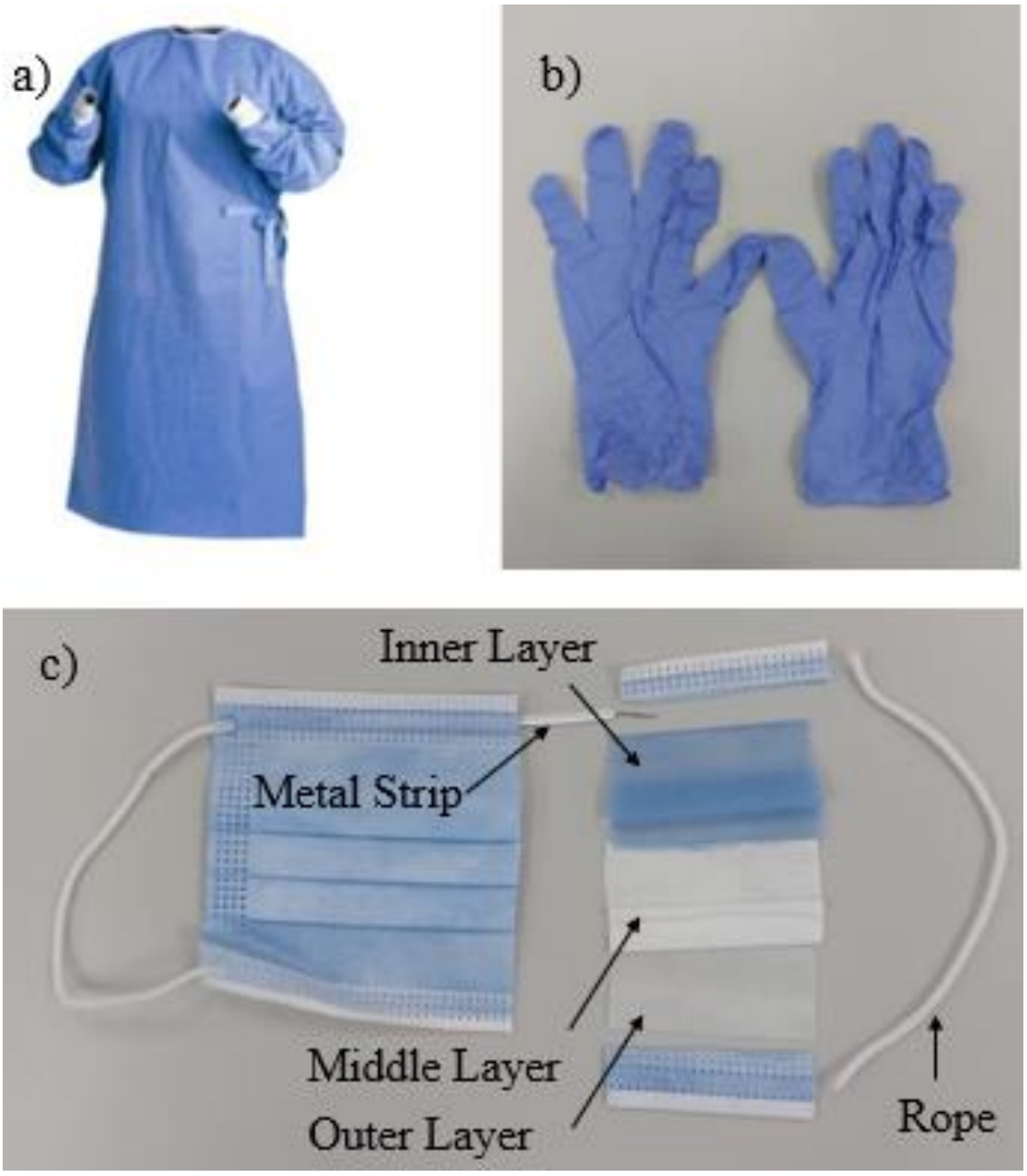

Figure 3.1 Photographs of medical waste samples used in this study: a) medical gown, b) nitrile glove, c) medical mask.

Samples were cut into pieces and dried for 24 hours at 105^{o}C. For combustion, pyrolysis, and fly ash characterization, square-shaped pieces with a size of 2x2 mm were cut from the original samples. Square-shaped pieces of 2x2 mm for gloves and 3x3 cm for mask and gown were cut for bottom ash characterization. Also, square-shaped pieces of 2x2 mm for mask and gown were cut for bottom ash analysis. After seeing no difference in ash, 3x3 cm particles were used for further analysis to decrease the sample preparation time. Prepared samples were shown in Figures 3.2-3.4.

In this thesis, four blends of medical waste have been prepared. The blend preparation and investigation process was constructed similarly to the methods used by Farokki et al. [149]. One blend was designed to represent the medical waste collected from hospitals' Covid-19 services. Other blends were prepared to investigate the synergistic effect of different medical wastes during co-combustion.

Figure 3.2 Nitrile glove samples cut under 2 mm.

Figure 3.3 Medical gown samples cut under 2 mm.

Figure 3.4 Face mask samples cut under 3 cm.

The medical staff regularly uses Personal Protective Equipment (PPE) in hospitals. Two masks and three pairs of gloves are used for each patient visit. For twelve patient visits, one gown is used by the medical staff unless any interaction contaminates it. The usage of PPE for each round is given in Table 3.1.

Table 3.1 Hospital COVID-19 service personal protective equipment usage amounts.

PPE	**Per patient**	**Per service round**	**Mass fraction in the blend (%)**
Glove	6	72	60
Gown	1/12	1	20
Mask	2	24	20

In the study, four different blends were prepared. The first one was prepared according to the above explanation of the actual usage amount in the hospitals. In other blends, only two kinds of samples were used to investigate their effects on each other at determined weight ratios. Blend compositions were given in Table 3.2 as corresponding weight ratios.

Table 3.2 Weight percentages of the blend compositions used in this thesis.

Blend Designation	**Glove (GL) (%)**	**Gown (G) (%)**	**Mask (M) (%)**
GL60G20M20	60	20	20
G50M50	-	50	50
GL50G50	50	50	-
GL60G40	60	40	-

3.2 Personal Protective Equipment Waste Characterization

In this section, methodologies of the characterization methods, such as proximate analysis, ultimate analysis, and differential scanning calorimetry, are given.

3.2.1 Proximate Analysis

A thermogravimetric analyzer (TGA) is a well-known and widely adopted analyzer used for the characterization of the thermal behavior of different feedstocks under various thermal conditions. Proximate analysis was conducted by Perkin Elmer 4000 TGA located in METUWIND Composite Material Characterization Laboratory, which is shown in Figure 3.5. The TGA device has a compact ceramic furnace with gas flow controllers, a thermocouple to record the temperature, and a micro-scale able to weigh 10^{-6} mg to record the weight of the sample. The sample was heated to 105 ^{o}C at a 10 ^{o}C/min rate with a nitrogen flow of 100 ml/min at 2 bar pressure. The sample was kept in isothermal conditions for 5 minutes. After that, the temperature was first increased to 950 ^{o}C with previous conditions and decreased to 450 ^{o}C at a 20 ^{o}C/min cooling rate. From 450 ^{o}C sample was heated up to 950 ^{o}C at a 10 ^{o}C/min rate with an airflow of 100 ml/min at 2 bar pressure and held in isothermal conditions for 5 minutes.

3.2.2 Ultimate Analysis

Ultimate Analysis was carried out in MERLAB METU using LECO, CHNS-932 with a similar method used by [150,151]. The sample was placed into an autoloader and dropped into the high-temperature combustion furnace. The combustion gases were swept from the furnace, through scrubbing reagents, and onto the detection systems as they were released. IR detectors were used to detect carbon, hydrogen, and sulfur simultaneously. Nitrogen was measured using a thermal conductivity detection system.

3.2.3 Differential Scanning Calorimetry

DSC analysis was carried out with a Perkin Elmer DSC 4000 single furnace located in the METUWIND Composite Material Characterization Laboratory, shown in Figure 3.6, with a similar method used by [152]. The sample is placed inside a container and inserted into the analyzer with an identical empty container used as a reference.

Heating and cooling rates in this analysis were +10^{o}C/min and -10^{o}C/min, respectively, and the temperature range was between -50 ^{o}C and 200 ^{o}C. Initially, samples were held at -50^{o}C for 10 minutes and then heated to 200^{o}C. Samples were kept in isothermal conditions for 10 minutes and cooled to -50^{o}C. After that, samples were held at isothermal conditions for 10 minutes and heated to 200^{o}C.

3.3 Pyrolysis of Personal Protective Equipment

Pyrolysis was carried out by Perkin Elmer 4000 TGA coupled with Perkin Elmer Spectrum 2 in METUWIND Composite Material Characterization Laboratory, shown in Figure 3.5, with a similar method used by [152,153]. Medical waste samples were heated to 900^{o}C at a 10^{o}C/min rate with a nitrogen flow of 100ml/min at 2 bar pressure. The resulting gas composition was channeled through a heated pipe at 270 ^{o}C to avoid condensation inside the channel through the Spectrum 2 device for FTIR analysis.

3.4 Combustion of Personal Protective Equipment

Combustion was carried out by Perkin Elmer 4000 TGA coupled with Perkin Elmer Spectrum 2, with a similar method used by [152,153]. Medical waste samples were heated to 900^{o}C at a 10^{o}C/min rate with an airflow of 100ml/min at 2 bar pressure. The resulting gas composition was channeled through a heated pipe at 270 ^{o}C to

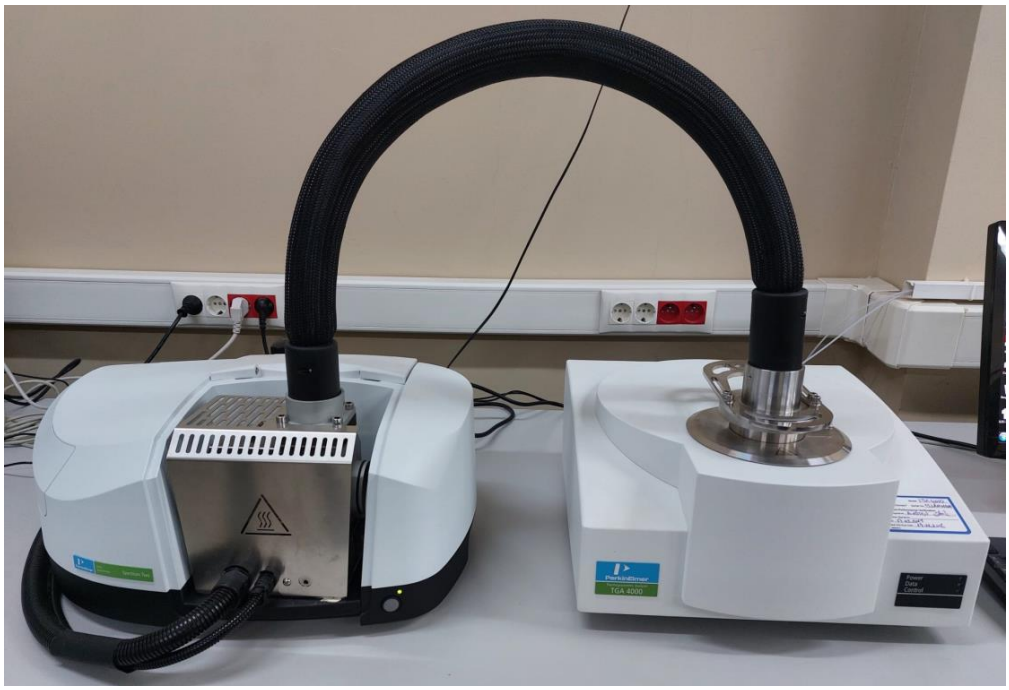

Figure 3.5 Thermogravimetric analyzer (TGA) (on the right side) connected to Spectrum 2 Fourier-Transform Infrared Spectrometer (FTIR) (on the left) at the METUWIND Composite Material Characterization Laboratory, METU.

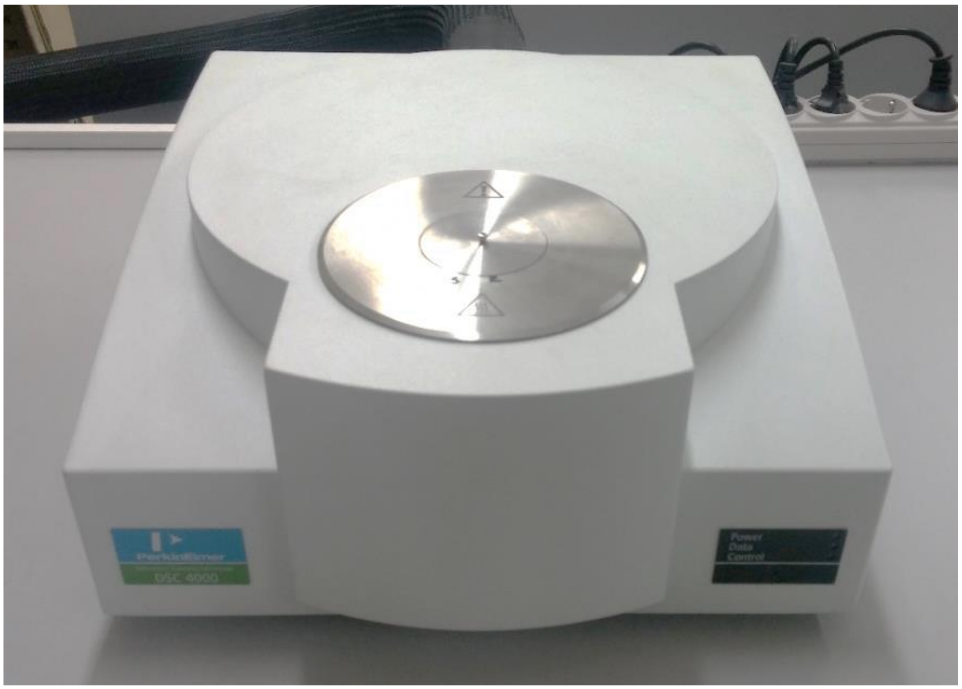

Figure 3.6 Differential Scanning Calorimetry (DSC) at the METUWIND Composite Material Characterization Laboratory, METU.

avoid condensation inside the channel through the Spectrum 2 device for FTIR analysis.

Prepared blends of the medical waste were examined with the same procedure as the one used for individual medical waste. Moreover, a weighted average of the DTG profiles was calculated using individual medical waste' DTG curves for the blends. The estimated profile was compared with the experimental DTG profiles from the burning of the blends.

3.5 Fourier Transform Infrared Spectroscopy

Fourier Transform Infrared Spectroscopy, or FTIR, is a highly valuable technique in verifying the identity of pure compounds and is widely adopted for determining organic and polymeric compositions [77,154]. The FTIR instrument sends infrared (IR) radiation with a wavelength range of approximately 10,000 to 100 cm^{-1} through a sample. As the radiation passes through the sample, some is absorbed and transmitted within. The absorption of IR radiation by sample molecules leads to energy conversion into rotational and/or vibrational motion, leading to stretching, bending, and twisting chemical bonds. This technique relies on identifying functional groups within molecules that exhibit specific vibrational patterns, either through stretching or bending, when exposed to particular wavelengths of light. These vibrational motions and their intensity (% transmission) are plotted against the frequency of light (measured in cm^{-1}) to generate an FTIR spectrum.

Certain regions of this spectrum, known as the fingerprint region, display distinct characteristics unique to the compound being analyzed. FTIR spectroscopy employs four sampling techniques: transmission, attenuated total reflection (ATR), specular reflection, and diffuse reflection. Additionally, the choice of infrared sources varies depending on the desired region of the IR spectrum to be examined. For the mid-IR region (5,000 – 400 cm^{-1}), silicon carbide (SiC) elements are commonly used, while

higher temperature sources like tungsten-halogen lamps are employed for the near-IR region (10,000 – 4,000 cm^{-1}).

In this thesis, the Perkin Elmer Spectrum 2 FTIR device, shown in Figure 3.2, is used for FTIR analysis. The FTIR device does not synchronize with TGA, so both devices were set and started manually at the same time. The absorption spectra were obtained with 32 scans between 4000 and 400 cm^{-1} with 4 cm^{-1} resolution.

3.6 Ash from Combustion of Personal Protective Equipment

For bottom ash production, medical waste samples were burned in a muffle furnace, shown in Figure 3.7, at 900^{o}C with a 10^{o}C/min heating rate under 5 L/min air flow at atmospheric pressure and kept in isothermal conditions for 10 minutes. The chemical composition of the resulting bottom ash was investigated by two different methods, namely SEM-EDX analysis and ICP-OES analysis[155].

Figure 3.7 Muffle furnace in Clean Combustion Technologies Laboratory, METU.

3.6.1 Scanning Electron Microscopy - Energy Dispersive X-Ray Spectroscopy

Scanning Electron Microscopy with Energy Dispersive X-Ray Spectroscopy (SEM-EDX) analysis was performed using QUANTA 400F Field Emission SEM. This analysis was performed at METU MERLAB. The bottom ash samples were attached to a carbon tape during SEM-EDX scanning, coated with gold and palladium for electrical conductivity, and readings were collected at least three random points. EDX is an analytical method used to determine a sample's elemental composition. The bottom ash samples are bombarded with high-energy electrons, causing the atoms in the ash to emit X-rays. Emitted X-rays are collected by a detector, which converts that information into electrical signals. The resulting spectrum shows the intensities of the X-rays as a function of their energies. Each element in the spectrum was identified from the peaks of that X-ray spectrum. The amount of each element in the sample is computed according to the intensity of the emitted characteristic X-ray. Since different atoms emit different amounts of X-ray, a correction was performed according to each element's atomic number, emissivity, and reflectivity. Random measurements taken from various parts of the sample surface were combined to calculate one overall value representing the final result. All of the collected measurements are given in Appendix E.

3.6.2 Inductively Coupled Plasma Optic Emission Spectroscopy

Prior to the ICP analysis, the microwave digestion of the PPE samples was performed using a Mars 6 240/50 series oven at a maximum power output of 3150W and magnetic frequency of 2455MHz. The four samples labeled *Gloves*, *Mask, Gown* & *GL60G20M20* were divided into duplicates (a, b) and then transferred into digestion vessels already containing 20ml of nitric acid (70%). Approximately 20mg of sample was added to each vessel. The digestion process was based on a 30-minute heating protocol based on ASTM D6349-13 with the following parameters: temperature

ramp of 25°C-200°C for two hours followed by a hold time of 10 minutes. The decomposition was achieved in the microwave oven at a power output of 1030-1800W.

After digestion was completed, the digestion vessels were opened, and 5ml of the digested leftovers were withdrawn and filtered using a 0.2μm syringe filter into ICP tubes. Afterward, the filtered samples were diluted at 50:50 (v/v) using 1M HNO_3 and ready for analysis. Inductively Coupled Plasma Optical Emission Spectrometry (ICP-OES) was used to analyze As, Hg, Mo, O, Se, Al, Ca, Co, Cr, Cu, Fe Mg, Mn, Ni, Pb, Zn, S, Au, Si, Ti elements at different frequencies, where the most suitable was selected to compute the results. The ICP was set to a plasma flow of 12 L/min, a nebulizer flow of 0.70 L/min, and a stabilization time of 15 seconds [156,157].

3.6.3 Slagging Performance

In order to evaluate the slagging performance of the bottom ash, conventional methods that Christy Vijay et al. [158] used are applied for both individual and blend analysis.

Base-to-acid ratio (B/A) is the ratio of basic and acidic compounds. Basic compounds decrease the ash melting temperature, while acidic compounds are known to increase that. The slagging inclination of ash is said to be low for B/A < 0.5, medium for 0.5 < B/A < 1.0, high for 1.0 < B/A < 1.75, and severe for B/A > 1.75 [159,160]. The formula below calculates the ratio, representing each oxide by its mass fractions.

$$B/A = \frac{m_{(Fe_2O_3)}+m_{(CaO)}+m_{(MgO)}+m_{(Na_2O)}+m_{(K_2O)}}{m_{(SiO_2)}+m_{(Al_2O_3)}+m_{(TiO_2)}} \quad (4)$$

3.7 Uncertainty Analysis

In experimental studies, the error is unavoidable. This error may arise from experimental setup, changing conditions of the experiment environment, or even human mistakes. Even though experimental error is inevitable, it can be predicted and minimized by proper setups and careful planning and investigation of the experimental data. For this purpose, uncertainty analyses for TGA and DSC were provided in the following subsections.

3.7.1 Thermogravimetric Analyzer

A thermogravimetric analyzer was used for proximate analysis, pyrolysis, and combustion. Perkin Elmer 4000 TGA device has a maximum operating temperature of 1000 ^{o}C, temperature accuracy of ±1 ^{o}C, and temperature precision of ±0.8 ^{o}C, with a balance accuracy of ±0.02% and precision of ±0.01% specified by the manufacturer. In order to minimize the error in the experiment, calibration of the device is essential. After each experiment, some residue was left on the crucible and should be cleaned properly before each use to avoid any error. At the beginning of the experiment, a crucible was placed, and its weight should be taken as tare weight. After the sample was placed, the sample weight was taken. Gas flow was supplied from the beginning to avoid any sudden changes. Half an hour of waiting time was taken so that the weight sensors stabilized after placing the crucible each time.

Also, each analysis was run at least twice, and the data set closer to the average of those sets was taken in the results section.

3.7.2 Differential Scanning Calorimetry

The Perkin Elmer DSC 4000 device was used for differential scanning calorimetry analysis and had an operating temperature between -100 ^{o}C and 450 ^{o}C, with a temperature accuracy of ±0.1 ^{o}C and precision of ±0.02 ^{o}C. Thermocouple-based

chrome alloy (90% Nickel / 10% Chromium) discs were used as temperature sensors. The device was calibrated with running high-purity reference materials with known temperature and energy transition for temperature and heat flow.

CHAPTER 4

RESULTS AND DISCUSSION

This chapter presents and discusses the results of the previously described analyses. In section 4.1, the results of the characterization analyses are provided. Selected PPEs are produced by a variety of manufacturers all over the world, with slight differences in their production process and ingredients. Proximate and ultimate analyses with differential scanning calorimetry results are compared with the literature data to confirm the used PPE represents the intended equipment. Sections 4.2 and 4.3 provide the results of thermochemical processes, pyrolysis, and combustion. In these sections, the derivative thermogravimetry graphs and FTIR spectrums are investigated. Especially in section 4.3, constructed blends are investigated for PPE's effect on each other. Finally, in section 4.4, SEM-EDX and ICP-OES results performed on the ash obtained from combustion are provided. A comparison of these methods provides essential information about the bottom ash of PPE and the slagging inclination of these samples. The experimental matrix is given in Table 4.1.

4.1 Personal Protective Equipment Waste Characterization

Selected PPE are characterized by proximate, ultimate, and DSC analyses, and their results are presented in this section.

4.1.1 Proximate and Ultimate Analyses of Personal Protective Equipment

Proximate and Ultimate Analysis results are given in Table 4.2. Glove samples have 1.6% moisture, 2.6% fixed carbon, and 4.3% ash residue, with a very high amount of volatile matter at 91.5%.

Table 4.1 Experimental matrix.

Process			Explanation		
Sample Preparation			Drying and cutting		
Characterization Analyses			**Experimental Setup**	**Temperature & Heating Rate**	**Atmosphere**
	Proximate Analysis		Perkin Elmer TGA 4000	950-450-950 ºC & +- 10 ºC/min	100 ml/min Nitrogen
	Differential Scannina		Perkin Elmer DSC 4000	-50-200 ºC & +- 10 ºC/min	20 ml/min Nitrogen
				Outsourced Facility	
	Ultimate Analysis		LECO, CHNS-932	METU MERLAB	
Pyrolysis Experiments			**Experimental Setup**	**Temperature & Heating Rate**	**Atmosphere**
			Perkin Elmer TGA 4000 Perkin Elmer Spectrum 2 FTIR	900 ºC & 10 ºC/min 270 ºC constant	100 ml/min Nitrogen
Combustion Experiments			**Experimental Setup**	**Temperature & Heating Rate**	**Atmosphere**
			Perkin Elmer TGA 4000 Perkin Elmer Spectrum 2 FTIR	900 ºC & 10 ºC/min 270 ºC constant	100 ml/min Air
Ash Characterization Analyses			**Experimental Setup**	**Temperature & Heating Rate**	**Atmosphere**
	Ash Production		Muffle Furnace	900 ºC & 10 ºC/min	5 L/min Air
				Outsourced Facility	
	Elemental Analysis	*SEM-EDX*	Quanta 400F Field Emission SEM	METU MERLAB	
		ICP-OES	Mars 6 240/50 Oven & ICP-OES	University of Limerick	

Table 4.2 Proximate and ultimate analysis of Personal Protective Equipments.

Parameter	**Glove**	**Gown**	**Mask**
Proximate Analysis, wt.% db			
Moisture	1.6	-	0.1
Volatiles	91.5	98.7	98.7
Fixed Carbon	2.6	0.4	0.9
Ash	4.3	0.9	0.3
Ultimate Analysis, wt.% daf			
C	71.5	82.2	80.2
H	8.6	14.7	14.0
N	6.9	0.5	0.1
O[a]	13.0	2.6	5.7
S	<0.1	<0.1	<0.1

[a] by difference

In the previous studies in Table 2.1, volatile matter was between 87 and 94%, so 91.5% for nitrile gloves was expected. Gown and mask results were similar in both analyses since they were made with the same material and similar production techniques. As seen in Table 4.2, both samples have 98.7 % volatile matter and minimal amounts of fixed carbon, 0.4% for the gown and 0.9% for mask, and ash content, as 0.9% for gown and 0.3% for mask. In Table 2.1, previous studies have reported mostly more than 99% volatile matter for polypropylene and more than 96% for face masks. From that comparison, it is safe to say that the used face mask and medical gown proximate analyses confirm those studies.

The ultimate analysis investigated the samples' C, H, O, N, and S content. All the samples have almost no amount of sulfur. Glove samples have 71.5% carbon, 8.6%

hydrogen, 6.9% nitrogen, and 13.0% oxygen. Gown and mask samples have around 80% carbon, 14% hydrogen, 0.5% nitrogen, and approximately 2 to 5% oxygen. All the ultimate analysis results are similar to the literature data in Table 2.1, except for a slight decrease of around 5% in carbon content, with a similar increase in the oxygen content of gown and mask samples.

4.1.2 Differential Scanning Calorimetry of Personal Protective Equipments

In DSC Analysis, Glass Transition, Crystallization, and Melting Temperatures were investigated, and results are presented in Table 4.3. The glove has only a glass transition temperature of -15 ^{o}C and no crystallization and melting temperatures. Gown and glove samples behave similarly at -18 and -20 ^{o}C for glass transition temperature, 110 and 120 ^{o}C for crystallization temperature, and 160 ^{o}C for melting temperature. All three temperatures for each sample, glass transition, crystallization, and melting temperature, were consistent with the literature data in Section 2.3.2. Gown and mask samples have slightly higher glass transition temperatures when compared to polypropylene, which indicates the production process has slightly altered material properties.

Table 4.3 Differential Scanning Calorimetry analysis of Personal Protective Equipments.

	Glass Transition Temperature ^{o}C	**Crystallization Temperature ^{o}C**	**Melting Temperature ^{o}C**
Glove	-15	-	-
Gown	-18	110	160
Mask	-20	120	160

4.2 Pyrolysis of Personal Protective Equipments

Pyrolysis of PPE and their blends was conducted using a thermogravimetric analyzer (TGA), and the corresponding TG-DTG curves are presented in Figure 4.1 and Figure 4.2. Figure 4.1 shows that all waste samples represented a single decomposition stage with a pronounced peak. Table 4.4 shows the characteristic temperatures for the decomposition of the samples, namely, decomposition (T_d), peak (T_p), and end of decomposition (T_{ed}) temperatures.

Compared to the literature data presented in Section 2.4 [62–65,90,115,116], gloves have similar decomposition and peak temperatures at 300 ^oC and 445 ^oC, respectively, with a slightly higher end-of-decomposition temperature of 523 ^oC. In comparison, it was reported up to 500 ^oC for NBR in the literature [105–113]. The gown and mask have similar decomposition temperatures to literature data on face masks [51,52,54–62,91,103,104] and polypropylene [43–50,88–102] in Section 2.4, at 320 ^oC, slightly lower peak temperature at 440 ^oC for the gown and 430 ^oC for the mask, and slightly lower end-of-decomposition temperature at 468 ^oC for gown and 465 ^oC for mask.

Table 4.4 Pyrolysis and combustion characteristics temperatures of Personal Protective Equipments.

	Pyrolysis			**Combustion**				
	T_d (^oC)	**T_p (^oC)**	**T_{ed} (^oC)**	**T_i (^oC)**	**T_{p1} (^oC)**	**T_{p2} (^oC)**	**T_{p3} (^oC)**	**T_b (^oC)**
Glove	300	445	523	240	420	450	510	564
Gown	320	440	468	220	385	-	-	398
Mask	320	430	465	238	362	-	-	390

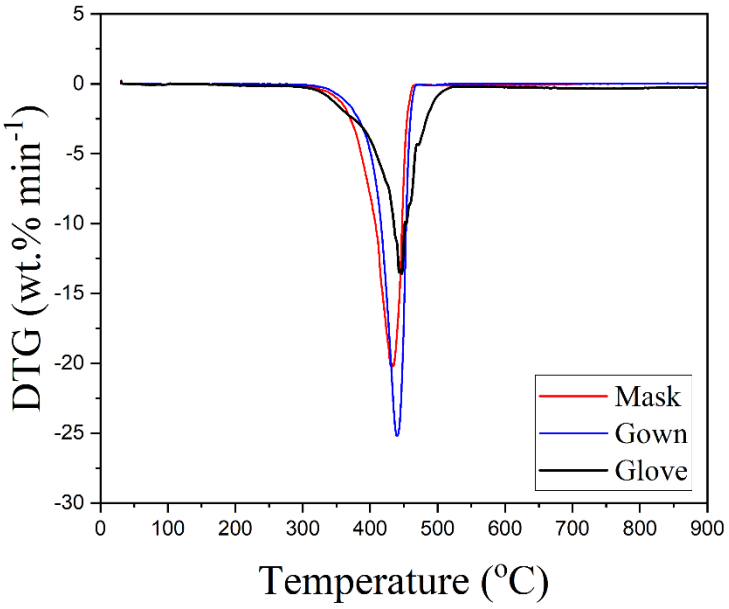

Figure 4.1 Pyrolysis DTG profiles of individual Personal Protective Equipments

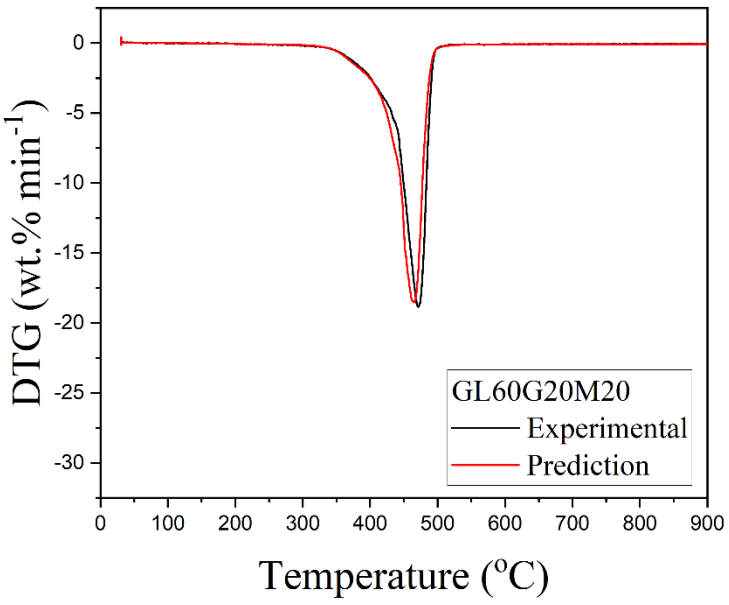

Figure 4.2 Pyrolysis DTG profile comparison of experimental and predicted GL60G20M20

With the acquired DTG profiles for individual samples, a prediction for blend GL60G20M20 has been made according to the weight percentage of the selected wastes in the blends. In Fig. 4.2, GL60G20M20 and its prediction are shown. All the characteristic temperatures, decomposition temperature, peak temperature, and end-of-decomposition temperature, were as predicted; therefore, no synergistic effect was observed in the co-pyrolysis of face mask, medical gown, and nitrile glove.

Gaseous emissions during pyrolysis were examined with TG-FTIR analysis, and the results are presented in Figures 4.3-4.6. Mask and gown samples' gaseous emissions are remarkably similar since their raw materials and production techniques are almost identical. For both samples, peaks at 2956 cm^{-1} and 2910 cm^{-1} were identified as characteristics associated with the -OH groups of the main functional groups that refer to polypropylene non-woven fabrics, and C-H stretch present in CH_2OH group that typically the peak of filter paper [52], at 2372 cm^{-1} and 2308 cm^{-1} as CO_2, at 1460 cm^{-1} and 1377 cm^{-1} as alkanes C-H stretching and bending bands of CH_2 and CH_3, respectively [161], and peak at 1027 cm^{-1} as C-H bend of CH_3 [162]. The fluctuations around 808 cm-1 indicate CH_3, CH_2, C-C, and C-CH_3 vibration bonds.

The presence of CH_2 and CH indicates that the random scission mechanism was primarily active. In contrast, the presence of CH_3 suggests that the side group scission mechanism was also present during the pyrolysis of polypropylene-based PPE. The small amounts of carbon bonds in C-C and C-CH_3 indicate some parts where random scission was not dominant. On the other hand, in blend GL60G20M20, C-C, and C-CH_3 bonds were not encountered, meaning that random scission was more dominant in blend pyrolysis.

For glove samples, peaks at 2933 cm^{-1} and 2867 cm^{-1} were identified as =C-H stretch [162], 2358 cm-1 and 2320 cm-1 as CO_2, and 1029 cm^{-1} as C-H bend of CH_3 [162]. The presence of =C-H indicates the monomer reversion mechanism was active, and the butadiene group was depolymerized at first. C-H bend and CH_3 indicate random scission, and side-group scission mechanisms are also present.

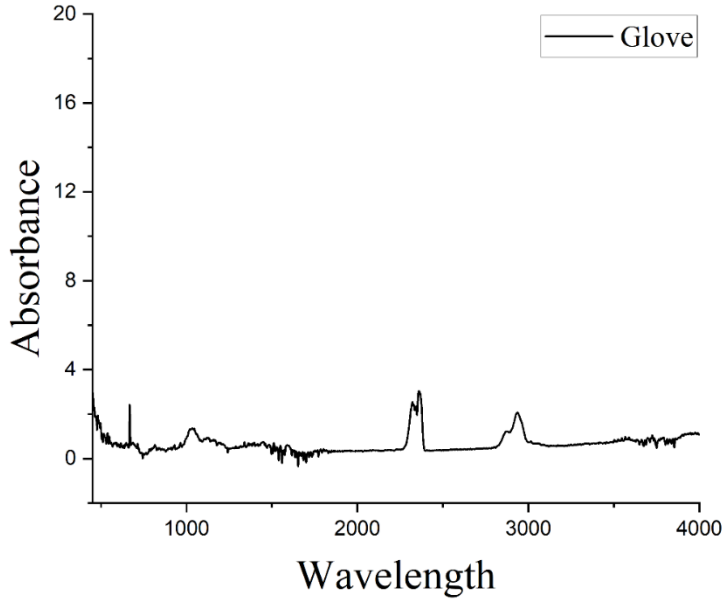

Figure 4.3 FTIR spectrum of the glove in pyrolysis conditions

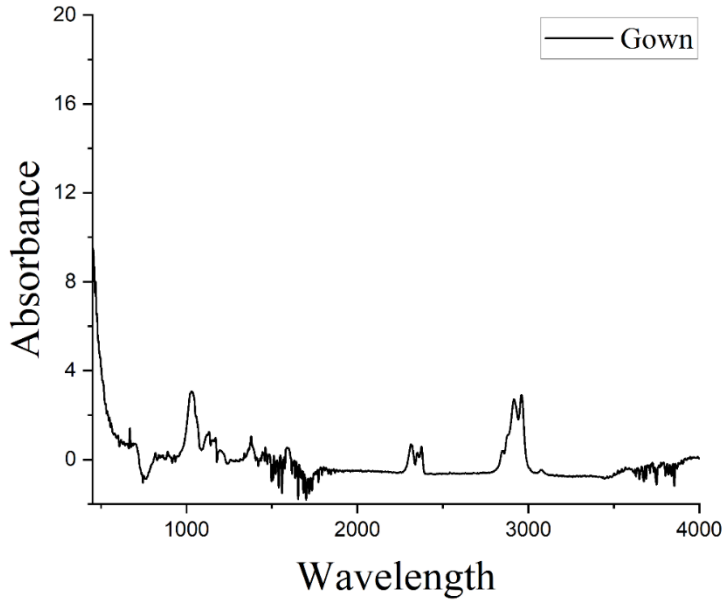

Figure 4.4 FTIR spectrum of the gown in pyrolysis conditions

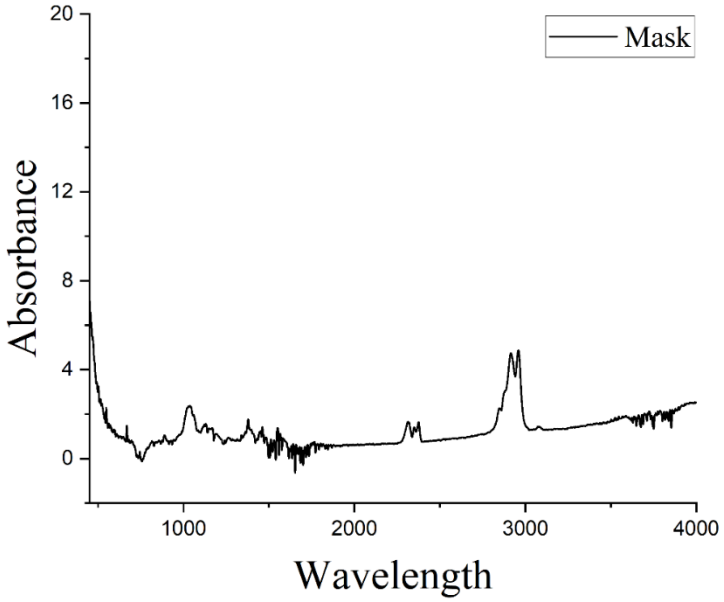

Figure 4.5 FTIR spectrum of mask in pyrolysis conditions

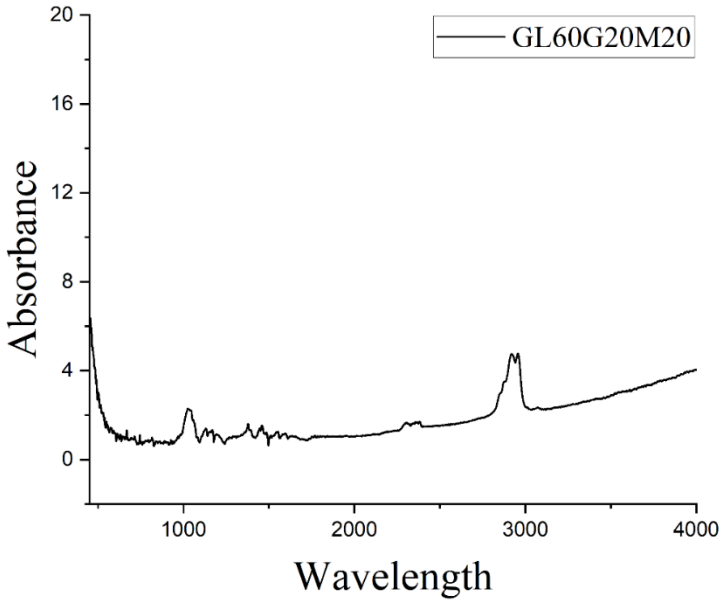

Figure 4.6 FTIR spectrum of GL60G20M20 in pyrolysis conditions

Similar to DTG profile comparison for blend analysis, blend GL60G20M20 emissions during pyrolysis are also compared with the individual results of the PPE. In the GL60G20M20 pyrolysis emissions, all the identified peaks were the same with the samples' separate analyses, and no unexpected gas emissions were found.

4.3 Combustion of Personal Protective Equipment

Combustion of medical wastes and their blends was conducted using a thermogravimetric analyzer (TGA), and the corresponding TG-DTG curves were presented in Figure 4.7-4.11. Figure 4.7 shows the DTG profiles of individual wastes in this study. Figure 4.7 shows the combustion characteristic temperatures of the samples, ignition temperature (T_i), peak temperatures (T_p), and burnout temperature (T_b), which are also presented in Table 4.4.

As in the pyrolysis section, the mask and gown had one peak in their DTG profile, as shown in Figure 4.7, representing a single combustion stage, while the glove had three distinct peaks representing three combustion stages.

Combustion characteristic temperatures in Table 4.4 were in good agreement with the literature data presented in Section 2.5 [51,53,93,94,97,102,103,114,115,128–132]. The glove has an ignition temperature of 240 ^{o}C, three peak temperatures at 420, 450, and 510 ^{o}C, and a burnout temperature of 564 ^{o}C. The gown has an ignition temperature of 220 ^{o}C, a peak temperature of 385 ^{o}C, and a burnout temperature of 398 ^{o}C. The mask has an ignition temperature of 238 ^{o}C, a peak temperature of 362 ^{o}C, and a burnout temperature of 390 ^{o}C. Indicated by the three distinct peak temperatures, nitrile glove exhibits three combustion stages. In the first peak, primarily, the volatile release is expected. In the second and third peaks, monomers in nitrile, acrylonitrile and butadiene, undergo combustion. The slight differences in combustion characteristic temperatures encountered can be attributed to factors such as raw material quality and differences in production techniques.

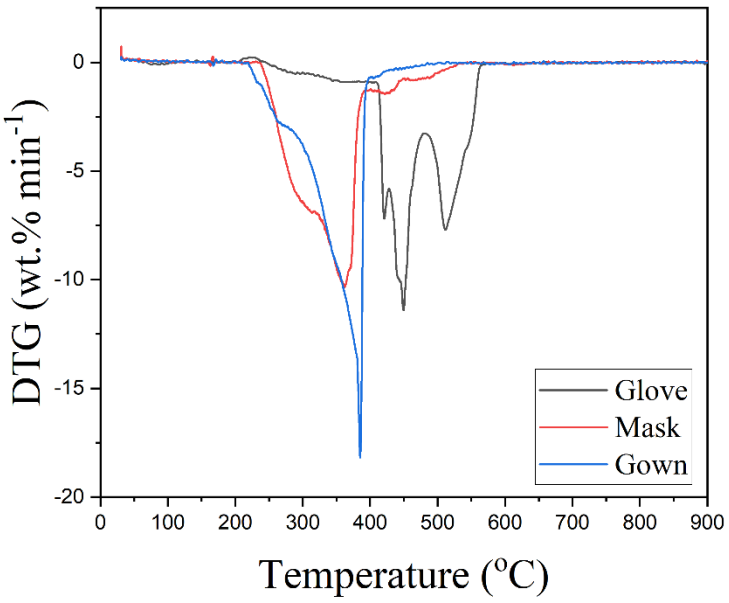

Figure 4.7 Combustion DTG profiles of individual Personal Protective Equipments

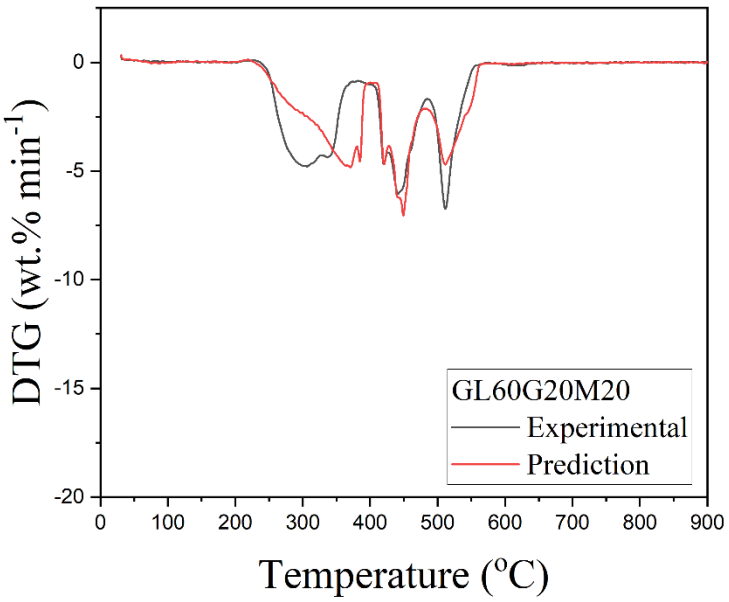

Figure 4.8 Combustion DTG profile comparison of experimental and predictions of GL60G20M20

With the acquired DTG profiles, a prediction for blends has been made according to the weight percentage of the selected wastes in the blends. In Fig. 4.8, GL60G20M20 and its prediction were shown. As seen from the figure, peak, and burnout temperatures for polypropylene-based materials, mask and gown, have shifted to lower temperatures, with peak temperatures from 370°C to 305°C and burnout temperatures from 395°C to 370°C, indicating a synergistic effect. In order to understand the reason for that synergistic effect, other blends with only two samples were prepared. In blend G50M50, equal amounts of polypropylene-based materials have been used. In Fig. 4.9, G50M50 and its prediction were shown.

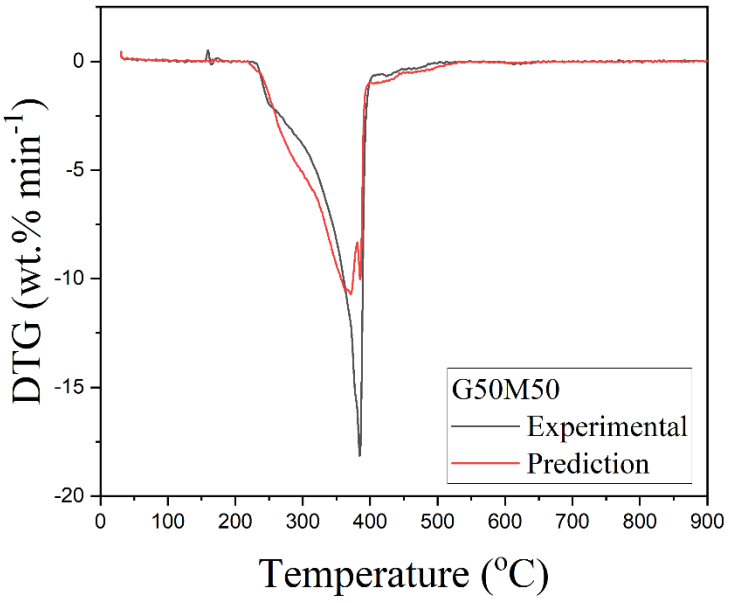

Figure 4.9 Combustion DTG profile comparison of experimental and predictions of G50M50

In the figure, all characteristic temperatures were similar to predictions, so a synergistic effect was not observed. In blend GL50G50, equal amounts of glove and gown samples have been used. In Fig. 4.10, GL50G50 and its prediction were given. In the figure, peak and burnout temperatures have shifted slightly to lower temperatures, peak temperatures from 385°C to 367°C, and burnout temperatures from 399°C to 390°C. In order to understand and verify whether that shift is due to

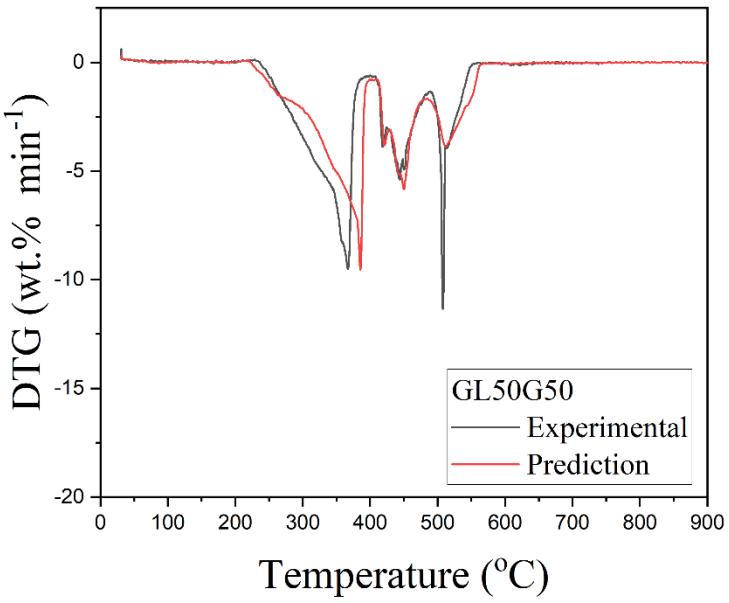

Figure 4.10 Combustion DTG profile comparison of experimental and predictions of GL50G50

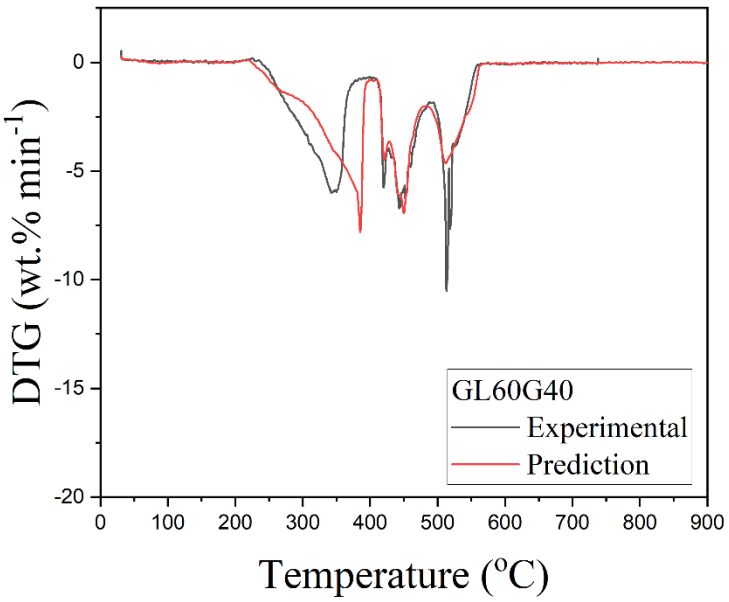

Figure 4.11 Combustion DTG profile comparison of experimental and predictions of GL60G40

nitrile glove addition, blend GL60G40 was prepared, with weight percentages of 60 for the glove and 40 for the gown.

In Fig. 4.11, GL60G40 and its prediction were shown. Compared to GL50G50 results, in GL60G40, the shift of peak and burnout temperatures to lower temperatures has increased, with peak temperature from 385^{o}C to 345^{o}C and burnout temperature from 399^{o}C to 385^{o}C.

These comparisons provide important insight into polypropylene and nitrile-based medical waste combinations. The DTG profiles revealed a significant shift in peak and burnout temperatures when varying proportions of nitrile gloves and polypropylene-based face masks and gowns were combined. As the nitrile glove ratio increases, the indicated shift also increases, allowing us to say nitrile glove has a synergistic effect on polypropylene-based PPE during combustion by decreasing peak and burnout temperatures. This synergistic effect can present itself by reducing residence time, harmful emissions, or slagging during the process. The following sections investigate gaseous emissions and ash compositions, which could shed light on the changes due to the synergistic effect on the final product.

Gaseous emissions during combustion were examined with FTIR analysis, and the results are presented in Figure 4.12-4.15. As was in the pyrolysis analysis section, results were presented for mask and gown samples together. The peaks at 2950 cm^{-1} and 2915 cm^{-1} were identified as characteristics associated with the -OH groups of the main functional groups referring to polypropylene non-woven fabrics, and C-H stretch present in CH_2OH group that typically the peak of filter paper [52], at 2300 cm^{-1} and 1735 cm^{-1} C=O stretch [162] of CO_2, at 1585 cm^{-1}, 1455 cm^{-1}, and 1377 cm^{-1} as alkanes C-H stretching and bending bands of CH_2 and CH_3 [161], at 1166 cm^{-1} and 1028 cm^{-1} as C-H bend of CH_3 [161–163]. Additionally, at minimal amounts, CH_3, CH_2, C-C, and C-CH_3 vibration bands were observed around 808 cm^{-1} [161,162].

The presence of CH_2 and CH indicates that the random scission mechanism was present, but the presence of C-C and C-CH_3 suggests that not all the carbon bonds

were broken, and at some minor parts, random scission was not dominant. Also, the presence of CH_3 indicates that side-group scission was observed.

For glove samples, the peaks around 2917 cm^{-1} identified as alkane, =C-H stretch, and saturated aliphatic groups [63], at 2300 cm^{-1} as CO_2, at 2237 cm^{-1} as -C≡N stretching of nitrile group [164], around 1400 cm^{-1} as -C-H stretching and bending vibrations of CH_2, and CH_3 [63,164], at 1197 cm^{-1} as CH_2 bend [162], and around 900 cm^{-1} as =C-H butadiene group [164].

The presence of =C-H and CH_2 indicates both monomer reversion and random scission mechanisms were effective. First, the butadiene group was depolymerized, and then by random scission mechanism, carbon bonds were broken to form =C-H and CH_2. Also, the presence of -C≡N and CH_2 indicates monomer reversion was also active for the acrylonitrile part.

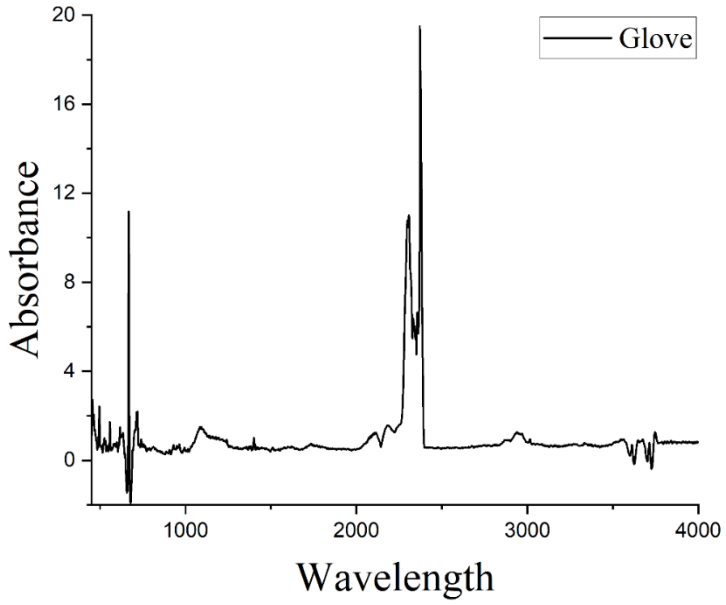

Figure 4.12 FTIR spectrum of the glove in combustion conditions

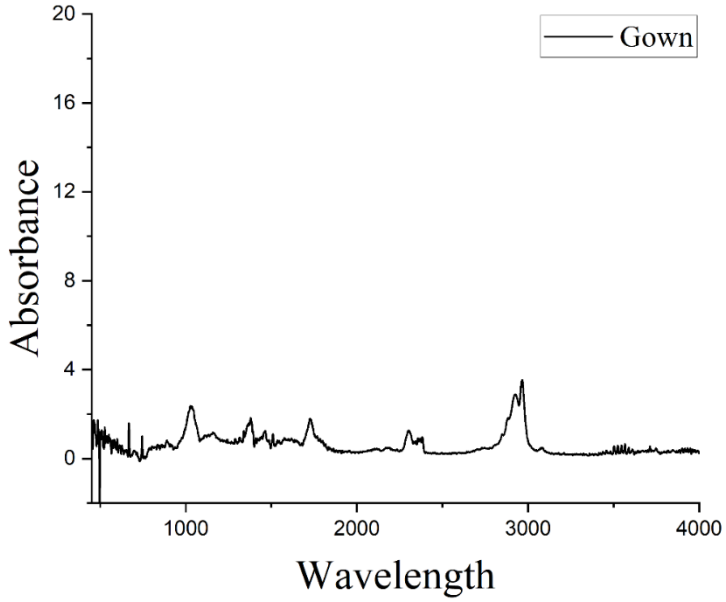

Figure 4.13 FTIR spectrum of the gown in combustion conditions

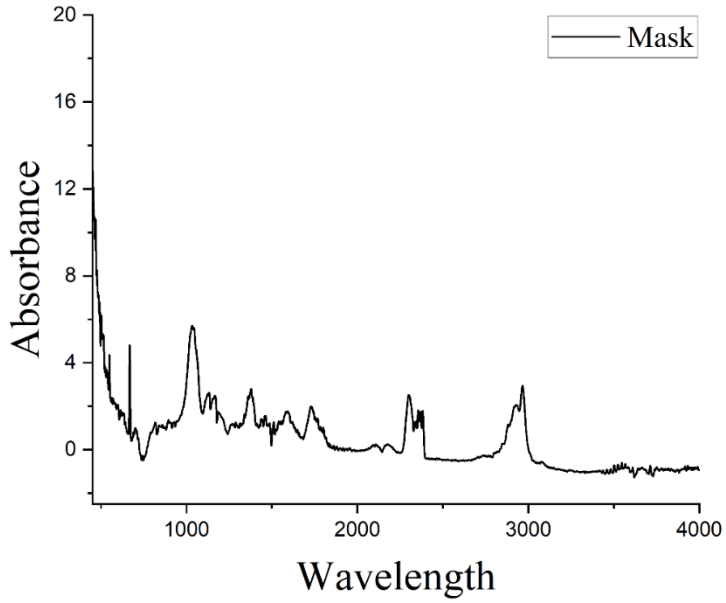

Figure 4.14 FTIR spectrum of the mask in combustion conditions

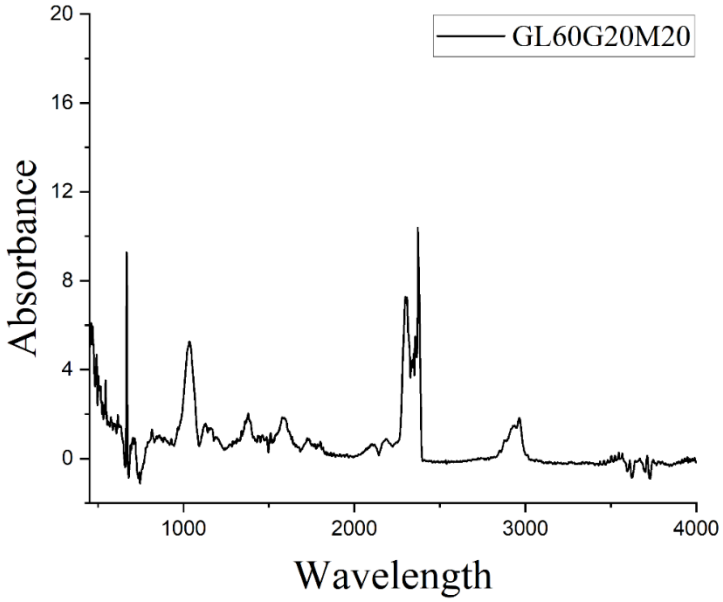

Figure 4.15 FTIR spectrum of GL60G20M20 in combustion conditions

After the random scission mechanism depolymerized the acrylonitrile group, carbon bonds were broken, resulting in the formation of CH_2, and by side-group scission -C≡N was formed. Compared to pyrolysis, monomer reversion and further cracking of bonds in acrylonitrile groups were clearer in combustion.

Similar to DTG profile comparison for blend analysis, blend GL60G20M20 emissions during combustion are also compared with the individual results of the PPE. In the GL60G20M20 combustion emissions, all of the identified peaks were the same with the separate analyses of the samples, and no unexpected gas emissions were found. Still, the intensity of the released gases decreased.

4.4 Ash from Combustion of Personal Protective Equipment Waste

The four medical waste samples (gloves, gowns, masks, and GL60G20M20) were assessed for elemental composition using ICP and EDX methods. Table 4.5

summarizes the results obtained for each sample and the technique utilized for element weight percentage in ash composition. In most of the samples, the Ti, Zn, and Ca concentrations were higher than the content of other metals according to both ICP-OES and SEM-EDX. The previous results have shown that medical waste samples contain high concentrations of alkali earth metals, e.g., Al, Ca, Fe, Mg (up to 315 g kg−1), and heavy metals such as Ag, Bi, Cr, Cu, Ni, Pb, Ti, and Zn (up to 121,411 mg kg^{-1}) [165]. The variety of heavy metals and corresponding concentrations were low compared to the literature [147,165]. Medical waste in Turkey probably contains low amounts of plastic, which typically integrates heavy metals as additives [166]. In addition, the Cr element found as highly toxic and present in high concentrations in previous studies was not observed in the present study [145].

The differences in Ti, Ca, Zn, S, and Al concentrations between results using ICP and EDX methods can be observed in Table 4.5. The ICP-OES determines the sample's average concentration of a specific element with well-distributed elements during digestion. At the same time, the SEM-EDX assesses a specific surface area of a sample for the presence of target elements and changes on the material surface [167]. The analysis results on the main elements (Ti, Ca, Zn, S, and Al) in the waste mixture ash characterized by different methods were comparable. This shows that, on average, the ash compounds in large concentrations can be accurately characterized using either EDX or ICP. The difference in both methods indicated that the material surface is inhomogeneous and, thus, can lead to measurement uncertainties using the EDX method. In addition, the results from the EDX method were treated with correction techniques, causing analysis uncertainties. The variations in Ti/Ca ratios of samples using ICP analysis were due to the pre-treatment of material using microwave acid digestion [168]. Higher amounts of Ti found in EDX results were expected since, during the production of PPE, TiO_2 was used as a dyeing agent.

Table 4.5 Ash elemental analysis results obtained with ICP-OES and SEM-EDX

	Glove (wt.%)		Gown (wt.%)		Mask (wt.%)		GL60G20M20 (wt.%)	
Element	**ICP**	**EDX**	**ICP**	**EDX**	**ICP**	**EDX**	**ICP**	**EDX**
Ti	5.78	20.79	16.36	34.98	10.91	33.85	15.84	13.81
Ca	12.52	12.2	5.15	5.07	13.18	13.14	11.87	7.95
Zn	9.17	11.42	-	-	-	-	8.91	7.57
S	8.42	9.16	1.69	0.24	-	-	7.82	5.76
Al	0.26	1.49	1.22	3.27	1.38	2.16	-	0.82
Other Elements	0.65	-	2.66	10.18	3.98	3.2	1.22	6.24

The concentration of sulfur for all samples was low according to both methods. However, the EDX method could underestimate the sulfur content as the SEM-EDX system is not precise for small element concentrations, especially when measurements are performed on inhomogeneous waste surfaces [169]. The differences in Ca concentrations measured by EDX and ICP-OES methods were related to the tendency of calcium to remain in the material during incineration [170]. This could lead to the inconsistent release of Ca into the flue gas under usual incineration temperatures [171]. Calcium could be present in the solid medical waste matrix as $CaCO_3$, $CaSO_4$, or CaO [172]. Heavy metals, e.g., Zn, are easily volatilized and condensed on the walls of furnaces during combustion [173]. Thus, the differences between ICP-OES and EDX methods were negligible.

Similarly, Ti and Al elements have high boiling points and tend to end up in the bottom ash during incineration. In contrast, a small fraction is released in a flue gas, leading to measurement uncertainty [145]. The Al was probably present as mullite ($3 \cdot Al_2O_3\ 2 \cdot SiO_2$) in gloves due to Si incorporation, whereas other samples contained Al as a corundum (Al_2O_3) [172]. This study recommends a complementary

use of both methods in the compositional characterization of medical waste inorganic matter.

It is widely accepted that these heavy metals may threaten human health and are the origin of lung and heart diseases. However, the results of the present work demonstrated that the concentrations of heavy metals, e.g., Zn, were within the EPA limits. This allows us to conclude that bottom ashes meet the waste acceptance criteria in US and EU countries [174]. The presence of major elements (Ti, Ca, Zn, and Al) in solid medical waste ash is encouraging for recycling and further use in the construction sector. Moreover, Zn amounts in the bottom ash are sparingly soluble, meaning that only small proportions of the total concentration can contaminate the groundwater and the air. This showed that the relatively negligible release of heavy metals during incineration and the remaining metal in the ash make the overall process harmless to the environment.

The base-to-acid ratios of the ash samples are given in Table 4.6. Glove and Mask ash samples have high slagging inclinations, 1.7 and 1.1, respectively, while gown ashes have very low, 0.2. In the co-combustion case, the slagging inclination of the blend GL60G20M20 was calculated by the weighted average of the individual sample results and compared with the actual blend sample. The base-to-acid ratio of GL60G20M20 was expected to be 1.3, which means high slagging, but found to be 0.6, meaning medium slagging. Therefore, the slagging was decreased in the co-combustion of the selected samples. This decrease in slagging increases energy recovery efficiency since slag formation on boiler walls or tubes decreases heat transfer efficiency. It also reduces maintenance costs that would rise due to extreme slag formation.

The base-to-acid ratio also represents the overall melting temperature of the ash composition. Basic compounds decrease the melting temperature, while acidic compounds are known to increase. By reducing the base-to-acid ratio, the overall melting temperature of the bottom ash has increased, which is beneficial for disposal, recycling, and reusing processes.

Table 4.6 Slagging inclination of the ash samples

Sample	Glove	Gown	Mask	GL60G20M20 (expected)	GL60G20M20 (experimental)
Base/Acid Ratio	1.7	0.2	1.1	1.3	0.6

CHAPTER 5

CONCLUSION

The COVID-19 pandemic has increased the focus on medical waste management, primarily on Personal Protective Equipment (PPE) waste. Due to the infectious nature of medical waste, high-temperature treatments are the most effective waste management procedure.

This study investigated the high-temperature characteristics and properties of PPE, such as gloves, gowns, and masks used in hospitals. Proximate, ultimate, and DSC analyses were performed to characterize the selected samples. To represent medical waste collected from COVID-19 services, blend GL60G20M20 was prepared according to the PPE usage amounts of healthcare workers. Since each material can affect the other during pyrolysis or combustion, blends, including only two pieces of equipment, were prepared, such as GL50G50, GL60G40, and G50M50. Individual and blend analyses of the selected equipment were performed under pyrolysis and combustion conditions. A thermogravimetric analyzer (TGA) coupled with a Fourier-transform infrared spectrometer (FTIR) was used for both analyses. The chemical composition of the bottom ash left after combustion was investigated with ICP-OES and SEM-EDX methods, and from the obtained composition of the ashes, slagging inclinations were calculated by their base-to-acid ratios.

The proximate, ultimate, and DSC analyses showed that selected samples have very similar characteristics with other brands and their respective raw materials by having more than 90% volatile matter, no amount of sulfur, and similar phase transition temperatures.

For blend analyses in pyrolysis and combustion, a prediction based on the individual analysis of the samples was prepared and compared with the experimental data of blend samples. The DTG and FTIR results showed that the pyrolysis process of the

medical waste blends was similar to the individual samples without the appearance of any synergistic effect. However, during combustion, the medical waste blend GL60G20M20 showed a synergistic effect on the polypropylene-based materials, causing a decrease in peak, from 370 ^{o}C to 305 ^{o}C, and burnout, from 395 ^{o}C to 370 ^{o}C, temperatures. Blends GL50G50, GL60G40, and G50M50 were prepared to investigate that effect. In G50M50, there was no difference between prediction and experimental data. However, in the combustion of blend GL50G50, the same synergistic effect with GL60G20M20 was observed, by a decrease in peak, from 385 ^{o}C to 367 ^{o}C, and burnout, from 399 ^{o}C to 390 ^{o}C, temperatures. When the nitrile glove amount in the blend was increased to 60%, in GL60G40, that same synergistic effect was increased as peak temperature from 385 ^{o}C to 345 ^{o}C, and burnout temperature from 399 ^{o}C to 385 ^{o}C. Also, during combustion, indicated by their FTIR spectrums, there were no significant changes in blend GL60G20M20 emissions except a slight decrease in emission intensity.

Both methods revealed similar results for ash compositions in the bottom ash analysis. ICP and EDX methods identified the same elements with some differences in element concentrations. After comparing both methods, this study suggests the complementary use of both techniques, EDX as a preliminary determination and ICP for further analysis.

The concentration of heavy metals in the blend GL60G20M20 was low in both methods, indicating that the process was harmless to the environment. The concentrations and qualitative characteristics of Ti, Ca, and Zn metals in bottom ash suggest their potential recycling or reuse in the construction industry. The study also shows that the slagging inclination was high for glove and mask samples, while for gown samples, slagging was low. In blend GL60G20M20, a similar prediction made in DTG profiles was also made for slagging inclination. Results showed that, while predictions implied high slagging potential, the slagging potential was decreased to lower medium regions in blend combustion.

From the mentioned results, it is clear that understanding the synergistic effects of waste blends is important. The observed decrease in peak and burnout temperatures in combustion highlights the complex interactions between waste components, especially between nitrile gloves and polypropylene-based medical gowns and face masks. The decrease in ash slagging inclination shows that energy recovery in rotary kiln is more efficient in the blended case, and damage to the equipment caused by slagging is decreased. This study offers opportunities for optimizing energy recovery from medical waste on a fundamental basis. Adaptation of more medical waste samples, a larger scale investigation, and further investigation of gaseous emissions are still required to further optimize this process, which could reveal more environmentally sustainable practices.

REFERENCES

[1] CDC Museum COVID-19 Timeline | David J. Sencer CDC Museum | CDC n.d. https://www.cdc.gov/museum/timeline/covid19.html (accessed March 3, 2023).

[2] WHO Director-General's opening remarks at the media briefing on COVID-19 - 11 March 2020 n.d. https://www.who.int/director-general/speeches/detail/who-director-general-s-opening-remarks-at-the-media-briefing-on-covid-19---11-march-2020 (accessed February 20, 2023).

[3] World Health Organization. Coronavirus disease (COVID-19): How is it transmitted? n.d. https://www.who.int/news-room/questions-and-answers/item/coronavirus-disease-covid-19-how-is-it-transmitted (accessed May 11, 2022).

[4] If you've been exposed to the coronavirus - Harvard Health n.d. https://www.health.harvard.edu/diseases-and-conditions/if-youve-been-exposed-to-the-coronavirus (accessed July 4, 2023).

[5] WHO Coronavirus (COVID-19) Dashboard | WHO Coronavirus (COVID-19) Dashboard With Vaccination Data n.d. https://covid19.who.int/ (accessed March 3, 2023).

[6] Callaway E. The coronavirus is mutating - does it matter? Nature 2020;585:174–7. https://doi.org/10.1038/D41586-020-02544-6.

[7] Mahmoudnia A, Mehrdadi N, Golbabaei Kootenaei F, Rahmati Deiranloei M, Al-e-Ahmad E. Increased personal protective equipment consumption during the COVID-19 pandemic: An emerging concern on the urban waste management and strategies to reduce the environmental impact. J Hazard Mater Adv 2022;7:100109. https://doi.org/10.1016/J.HAZADV.2022.100109.

[8] Personal Protective Equipment - Overview | Occupational Safety and Health Administration n.d. https://www.osha.gov/personal-protective-equipment (accessed May 18, 2023).

[9] Health products policy and standards n.d. https://www.who.int/teams/health-product-policy-and-standards/assistive-and-medical-technology/medical-devices/ppe (accessed May 18, 2023).

[10] Choosing The Correct PPE | Environmental Health & Safety n.d. https://ehs.ucmerced.edu/researchers-labs/ppe/selection (accessed July 4, 2023).

[11] Surgical Gown (Nonwoven, disposable) – M | Africa Medical Supplies Platform n.d. https://amsp.africa/product/surgical-gown-nonwoven-disposable-m/ (accessed July 4, 2023).

[12] Zhao Z, Wu S, Liu Q, Xie J, Yang C, Wang F, et al. Recycling waste disposable medical masks in improving the performance of asphalt and asphalt mixtures. Constr Build Mater 2022;337:127621. https://doi.org/10.1016/J.CONBUILDMAT.2022.127621.

[13] Jung S, Lee S, Dou X, Kwon EE. Valorization of disposable COVID-19 mask through the thermo-chemical process. Chem Eng J 2021;405:126658. https://doi.org/10.1016/J.CEJ.2020.126658.

[14] Armijo PR, Markin NW, Nguyen S, Ho DH, Horseman TS, Lisco SJ, et al. 3D printing of face shields to meet the immediate need for PPE in an anesthesiology department during the COVID-19 pandemic. Am J Infect Control 2021;49:302–8. https://doi.org/10.1016/J.AJIC.2020.07.037.

[15] Hossain L, Maliha M, Barajas-Ledesma R, Kim J, Putera K, Subedi D, et al. Engineering laminated paper for SARS-CoV-2 medical gowns. Polymer (Guildf) 2021;222:123643. https://doi.org/10.1016/J.POLYMER.2021.123643.

[16] Personal protective equipment for COVID-19 n.d. https://www.who.int/teams/health-product-policy-and-standards/assistive-and-medical-technology/medical-devices/ppe/ppe-covid (accessed February 20, 2023).

[17] Mahmud TS, Ng KTW, Karimi N, Adusei KK, Pizzirani S. Evolution of COVID-19 municipal solid waste disposal behaviors using epidemiology-based periods defined by World Health Organization guidelines. Sustain Cities Soc 2022;87:104219. https://doi.org/10.1016/J.SCS.2022.104219.

[18] Chang SH. Plastic waste as pyrolysis feedstock for plastic oil production: A review. Sci Total Environ 2023;877:162719. https://doi.org/10.1016/J.SCITOTENV.2023.162719.

[19] Plastic pollution is growing relentlessly as waste management and recycling fall short, says OECD n.d. https://www.oecd.org/environment/plastic-pollution-is-growing-relentlessly-as-waste-management-and-recycling-fall-short.htm (accessed July 11, 2023).

[20] Chowdhury T, Chowdhury H, Rahman MS, Hossain N, Ahmed A, Sait SM. Estimation of the healthcare waste generation during COVID-19 pandemic in Bangladesh. Sci Total Environ 2022;811:152295. https://doi.org/10.1016/J.SCITOTENV.2021.152295.

[21] Benson NU, Bassey DE, Palanisami T. COVID pollution: impact of COVID-19 pandemic on global plastic waste footprint. Heliyon 2021;7:e06343. https://doi.org/10.1016/J.HELIYON.2021.E06343.

[22] Tesfaldet YT, Ndeh NT. Assessing face masks in the environment by means of the DPSIR framework. Sci Total Environ 2022;814:152859. https://doi.org/10.1016/J.SCITOTENV.2021.152859.

[23] Klemeš JJ, Fan Y Van, Jiang P. The energy and environmental footprints of COVID-19 fighting measures – PPE, disinfection, supply chains. Energy 2020;211:118701. https://doi.org/10.1016/J.ENERGY.2020.118701.

[24] Zevenhoven R, Karlsson M, Hupa M, Frankenhaeuser M. Combustion and Gasification Properties of Plastics Particles. Http://DxDoiOrg/101080/10473289199710464461 2011;47:861–70. https://doi.org/10.1080/10473289.1997.10464461.

[25] Dincer I, Rosen MA, Khalid F. 3.16 Thermal Energy Production. Compr Energy Syst 2018;3–5:673–706. https://doi.org/10.1016/B978-0-12-809597-3.00335-7.

[26] Klemeš JJ, Fan Y Van, Tan RR, Jiang P. Minimising the present and future plastic waste, energy and environmental footprints related to COVID-19. Renew Sustain Energy Rev 2020;127:109883. https://doi.org/10.1016/J.RSER.2020.109883.

[27] Chang SH. A Comparative Study of Batch and Continuous Bulk Liquid Membranes in the Removal and Recovery of Cu(II) Ions from Wastewater. Water Air Soil Pollut 2018;229:1–11. https://doi.org/10.1007/S11270-017-3659-Z/TABLES/1.

[28] Verma R, Vinoda KS, Papireddy M, Gowda ANS. Toxic Pollutants from Plastic Waste- A Review. Procedia Environ Sci 2016;35:701–8. https://doi.org/10.1016/J.PROENV.2016.07.069.

[29] Selvaranjan K, Navaratnam S, Rajeev P, Ravintherakumaran N. Environmental challenges induced by extensive use of face masks during COVID-19: A review and potential solutions. Environ Challenges 2021;3:100039. https://doi.org/10.1016/J.ENVC.2021.100039.

[30] Hartanto BW, Triastianti RD. Eco-friendly masks preferences during COVID-19 pandemic in Indonesia. Clean Responsible Consum 2022;4:100044. https://doi.org/10.1016/J.CLRC.2021.100044.

[31] Gorrasi G, Sorrentino A, Lichtfouse E. Back to plastic pollution in COVID times. Environ Chem Lett 2021;19:1–4. https://doi.org/10.1007/S10311-020-01129-Z/FIGURES/1.

[32] de Haan WP, Sanchez-Vidal A, Canals M. Floating microplastics and aggregate formation in the Western Mediterranean Sea. Mar Pollut Bull 2019;140:523–35. https://doi.org/10.1016/J.MARPOLBUL.2019.01.053.

[33] Saberian M, Li J, Kilmartin-Lynch S, Boroujeni M. Repurposing of COVID-19 single-use face masks for pavements base/subbase. Sci Total Environ 2021;769:145527. https://doi.org/10.1016/J.SCITOTENV.2021.145527.

[34] Tıbbi Atıkların Toplanması ve Bertarafı - Çevre Koruma ve Kontrol Dairesi Başkanlığı Web Sitesi n.d. https://cevre.ibb.istanbul/atik-yonetimi-mudurlugu-sube-mudurlugu/tibbi-atiklarin-toplanmasi-ve-bertarafi/ (accessed May 23, 2023).

[35] Kasapoğlu C. SYNTHESIS AND CHARACTERIZATION OF TPA LOADED MESOPOROUS CATALYSTS AND THEIR PERFORMANCE IN PYROLYSIS OF POLYPROPYLENE A THESIS SUBMITTED TO THE GRADUATE SCHOOL OF NATURAL AND APPLIED SCIENCES OF MIDDLE EAST TECHNICAL UNIVERSITY 2013.

[36] Rehman A, Habib R. PRODUCTION OF VALUABLE CHEMICALS FROM PLASTIC WASTES CONTAINING POLYETHYLENE AND POLYPROPYLENE A THESIS SUBMITTED TO THE GRADUATE SCHOOL OF NATURAL AND APPLIED SCIENCES OF MIDDLE EAST TECHNICAL UNIVERSITY 2019.

[37] Obali Z. SYNTHESIS OF ALUMINUM INCORPORATED MESOPOROUS CATALYSTS FOR PYROLYSIS OF POLYPROPYLENE A THESIS SUBMITTED TO THE GRADUATE SCHOOL OF NATURAL AND APPLIED SCIENCES OF MIDDLE EAST TECHNICAL UNIVERSITY 2010.

[38] Yalçin UE. PERFORMANCE OF TPA LOADED SBA-15 CATALYST IN POLYPROPYLENE DEGRADATION REACTION A THESIS SUBMITTED TO THE GRADUATE SCHOOL OF NATURAL AND

APPLIED SCIENCES OF MIDDLE EAST TECHNICAL UNIVERSITY n.d.

[39] Acrylonitrile butadiene rubber (nitrile / NBR rubber) 2015.

[40] Acrylonitrile-butadiene rubber (NBR) | RADO Gummi GmbH n.d. https://www.rado-rubber.com/specialities/nbr/ (accessed August 7, 2023).

[41] Çağatay O. RUBBER TOUGHENING OF PHENOLIC RESIN BY USING NITRILE RUBBER AND AMINO SILANE A THESIS SUBMITTED TO THE GRADUATE SCHOOL OF NATURAL AND APPLIED SCIENCES OF THE MIDDLE EAST TECHNICAL UNIVERSITY 2005.

[42] Nunes LJR, De Oliveira Matias JC, Da Silva Catalão JP. Introduction of Proximate Analysis. 2018.

[43] Galiwango E, A.Gabbar H. Synergistic interactions, kinetic and thermodynamic analysis of co-pyrolysis of municipal paper and polypropylene waste. Waste Manag 2022;146:86–93. https://doi.org/10.1016/J.WASMAN.2022.04.032.

[44] Li J, Ye X, Burra KG, Lu W, Wang Z, Liu X, et al. Synergistic effects during co-pyrolysis and co-gasification of polypropylene and polystyrene. Appl Energy 2023;336:120750. https://doi.org/10.1016/J.APENERGY.2023.120750.

[45] Li Y, Yellezuome D, Cai J, Tao S, Liu R. Insight into the synergistic performance during ex-situ catalytic co-pyrolysis of poplar sawdust and polypropylene over Fe-Ni/ZSM-5 for the enhancement of aromatics. Ind Crops Prod 2023;193:116249. https://doi.org/10.1016/J.INDCROP.2023.116249.

[46] Terry LM, Wee MXJ, Chew JJ, Khaerudini DS, Timuda GE, Aqsha A, et al. Co-pyrolysis of oil palm trunk and polypropylene: Pyrolysis oil composition and formation mechanism. South African J Chem Eng 2023;43:348–58.

https://doi.org/10.1016/J.SAJCE.2022.12.001.

[47] Jiang L, Zhou Z, Xiang H, Yang Y, Tian H, Wang J. Characteristics and synergistic effects of co-pyrolysis of microalgae with polypropylene. Fuel 2022;314:122765. https://doi.org/10.1016/J.FUEL.2021.122765.

[48] Hassibi N, Quiring Y, Carré V, Aubriet F, Vernex-Loset L, Mauviel G, et al. Analysis and control of products obtained from pyrolysis of polypropylene using a reflux semi-batch reactor and GC-MS/FID and FT-ICR MS. J Anal Appl Pyrolysis 2023;169:105826. https://doi.org/10.1016/J.JAAP.2022.105826.

[49] Chen R, Zhang S, Cong K, Li Q, Zhang Y. Insight into synergistic effects of biomass-polypropylene co-pyrolysis using representative biomass constituents. Bioresour Technol 2020;307:123243. https://doi.org/10.1016/J.BIORTECH.2020.123243.

[50] Azizi K, Keshavarz Moraveji M, Abedini Najafabadi H. Characteristics and kinetics study of simultaneous pyrolysis of microalgae Chlorella vulgaris, wood and polypropylene through TGA. Bioresour Technol 2017;243:481–91. https://doi.org/10.1016/J.BIORTECH.2017.06.155.

[51] Brillard A, Kehrli D, Douguet O, Gautier K, Tschamber V, Bueno MA, et al. Pyrolysis and combustion of community masks: Thermogravimetric analyses, characterizations, gaseous emissions, and kinetic modeling. Fuel 2021;306:121644. https://doi.org/10.1016/J.FUEL.2021.121644.

[52] Yousef S, Eimontas J, Striūgas N, Abdelnaby MA. Pyrolysis kinetic behaviour and TG-FTIR-GC–MS analysis of Coronavirus Face Masks. J Anal Appl Pyrolysis 2021;156:105118. https://doi.org/10.1016/j.jaap.2021.105118.

[53] Manić N, Janković B, Dragoslava Stojiljković ·, Angelopoulos P, Radojević M. Thermal characteristics and combustion reactivity of coronavirus face masks using TG-DTG-MS analysis. J Therm Anal Calorim 2022;147:10131–

43. https://doi.org/10.1007/s10973-022-11358-9.

[54] Hooda S, Lanjewar R, Mondal P. In-depth study of kinetics, thermodynamics, and reaction mechanism of catalytic pyrolysis of disposable face mask using spent adsorbent based catalysts. J Energy Inst 2023;108:101247. https://doi.org/10.1016/J.JOEI.2023.101247.

[55] Nawaz A, Kumar P. Thermal degradation of hazardous 3-layered COVID-19 face mask through pyrolysis: Kinetic, thermodynamic, prediction modelling using ANN and volatile product characterization. J Taiwan Inst Chem Eng 2022;139:104538. https://doi.org/10.1016/J.JTICE.2022.104538.

[56] Hou Y, Feng Z, He Y, Gao Q, Ni L, Su M, et al. Co-pyrolysis characteristics and synergistic interaction of bamboo residues and disposable face mask. Renew Energy 2022;194:415–25. https://doi.org/10.1016/J.RENENE.2022.05.111.

[57] Occasi G, De Angelis D, Scarsella M, Tammaro M, Tuccinardi L, Tuffi R. Recovery material from a new designed surgical face mask: A complementary approach based on mechanical and thermo-chemical recycling. J Environ Manage 2022;324:116341. https://doi.org/10.1016/J.JENVMAN.2022.116341.

[58] Lee SB, Lee J, Tsang YF, Kim YM, Jae J, Jung SC, et al. Production of value-added aromatics from wasted COVID-19 mask via catalytic pyrolysis. Environ Pollut 2021;283:117060. https://doi.org/10.1016/J.ENVPOL.2021.117060.

[59] Xu W, Liu J, Ding Z, Fu J, Evrendilek F, Xie W, et al. Dynamic pyrolytic reaction mechanisms, pathways, and products of medical masks and infusion tubes. Sci Total Environ 2022;842:156710. https://doi.org/10.1016/J.SCITOTENV.2022.156710.

[60] Wang C, Zou R, Lei H, Qian M, Lin X, Mateo W, et al. Biochar-advanced thermocatalytic salvaging of the waste disposable mask with the production

of hydrogen and mono-aromatic hydrocarbons. J Hazard Mater 2022;426:128080. https://doi.org/10.1016/J.JHAZMAT.2021.128080.

[61] Montero-Calderón C, Tacuri R, Solís H, De-La-Rosa A, Gordillo G, Araujo-Granda P. Masks thermal degradation as an alternative of waste valorization on the COVID-19 pandemic: A kinetic study. Heliyon 2023;9:e13518. https://doi.org/10.1016/J.HELIYON.2023.E13518.

[62] Panchal N, Vinu R. Resource recovery from discarded COVID-19 PPE kit through catalytic fast pyrolysis. J Anal Appl Pyrolysis 2023;170:105870. https://doi.org/10.1016/J.JAAP.2023.105870.

[63] Mishra RK, Iyer JS, Mohanty K. Conversion of waste biomass and waste nitrile gloves into renewable fuel. Waste Manag 2019;89:397–407. https://doi.org/10.1016/J.WASMAN.2019.04.032.

[64] Gerasimov G, Khaskhachikh V, Kornilieva V, Tarasov G. Study of Pyrolysis of Components and Mixture of Medical Waste. Chem Eng Trans 2019;76:1423–8. https://doi.org/10.3303/CET1976238.

[65] Kumar Mishra R, Mohanty K. Co-pyrolysis of waste biomass and waste plastics (polystyrene and waste nitrile gloves) into renewable fuel and value-added chemicals. Carbon Resour Convers 2020;3:145–55. https://doi.org/10.1016/J.CRCON.2020.11.001.

[66] Majewsky M, Bitter H, Eiche E, Horn H. Determination of microplastic polyethylene (PE) and polypropylene (PP) in environmental samples using thermal analysis (TGA-DSC). Sci Total Environ 2016;568:507–11. https://doi.org/10.1016/J.SCITOTENV.2016.06.017.

[67] Glass Transition Temperature (Tg) of Plastics - Definition & Values n.d. https://omnexus.specialchem.com/polymer-properties/properties/glass-transition-temperature (accessed July 9, 2023).

[68] Greene JP. Microstructures of Polymers. Automot Plast Compos 2021:27–37.

https://doi.org/10.1016/B978-0-12-818008-2.00009-X.

[69] What is the Glass Transition Temperature of Plastics? - PlasticRanger n.d. https://plasticranger.com/what-is-the-glass-transition-temperature-of-plastics/ (accessed July 9, 2023).

[70] Teh JW, Blom HP, Rudin A. A study on the crystallization behaviour of polypropylene, polyethylene and their blends by dynamic mechanical and thermal methods 1994.

[71] Sowinski P, Veluri S, Piorkowska E. Crystallization of Isotactic Polypropylene Nanocomposites with Fibrillated Poly(tetrafluoroethylene) under Elevated Pressure. Polymers (Basel) 2022;14. https://doi.org/10.3390/POLYM14010088/S1.

[72] Beuguel Q, Boyer SAE, Settipani D, Monge G, Haudin J-M, Vergnes B, et al. Crystallization behavior of polypropylene/graphene nanoplatelets composites n.d.

[73] Glass Transition Temperature (Tg) of Polymers n.d. https://www.protolabs.com/resources/design-tips/glass-transition-temperature-of-polymers/ (accessed July 9, 2023).

[74] Alneamah M, Almaamori M. Study of Thermal Stability of Nitrile Rubber/Polyimide Compounds. Int J Mater Chem 2015;5:1–3. https://doi.org/10.5923/j.ijmc.20150501.01.

[75] Acrylonitrile (Nitrile) Butadiene Rubber (NBR, Buna-N) :: MakeItFrom.com n.d. https://www.makeitfrom.com/material-properties/Acrylonitrile-Nitrile-Butadiene-Rubber-NBR-Buna-N (accessed July 9, 2023).

[76] Liu Q, Zhang J, Li R, Wu Y, Liu G, Liu L, et al. Study on the relationship between structure and acoustic performance of NBR composite materials. Polymer (Guildf) 2022;258:125284. https://doi.org/10.1016/J.POLYMER.2022.125284.

[77] Akgül A. INVESTIGATION OF BIOMASS AND BIOPLASTIC WASTES USING FAST HEATING RATE THERMOCHEMICAL PROCESSES 2022.

[78] Stauffer E, Dolan JA, Newman R. Chemistry and Physics of Fire and Liquid Fuels. Fire Debris Anal 2008:85–129. https://doi.org/10.1016/B978-012663971-1.50008-7.

[79] What is Pyrolysis? : USDA ARS n.d. https://www.ars.usda.gov/northeast-area/wyndmoor-pa/eastern-regional-research-center/docs/biomass-pyrolysis-research-1/what-is-pyrolysis/ (accessed June 19, 2023).

[80] Palmer R. Identification and Comparison. Encycl Forensic Sci Second Ed 2013:129–37. https://doi.org/10.1016/B978-0-12-382165-2.00092-1.

[81] Frau C, Ferrara F, Orsini A, Pettinau A. Characterization of several kinds of coal and biomass for pyrolysis and gasification. Fuel 2015;152:138–45. https://doi.org/10.1016/J.FUEL.2014.09.054.

[82] Hu Q, Cheng W, Mao Q, Hu J, Yang H, Chen H. Study on the physicochemical structure and gasification reactivity of chars from pyrolysis of biomass pellets under different heating rates. Fuel 2022;314:122789. https://doi.org/10.1016/J.FUEL.2021.122789.

[83] Saber M, Nakhshiniev B, Yoshikawa K. A review of production and upgrading of algal bio-oil. Renew Sustain Energy Rev 2016;58:918–30. https://doi.org/10.1016/J.RSER.2015.12.342.

[84] Zhang Y, Chen P, Liu S, Peng P, Min M, Cheng Y, et al. Effects of feedstock characteristics on microwave-assisted pyrolysis – A review. Bioresour Technol 2017;230:143–51. https://doi.org/10.1016/J.BIORTECH.2017.01.046.

[85] Magalhaes D. Investigation of alternative biomass fuels and Turkish lignites at high heating rate pyrolysis and combustion conditions 2021.

[86] Toscano Miranda N, Lopes Motta I, Maciel Filho R, Wolf Maciel MR. Sugarcane bagasse pyrolysis: A review of operating conditions and products properties. Renew Sustain Energy Rev 2021;149:111394. https://doi.org/10.1016/J.RSER.2021.111394.

[87] Šesták J. THERMOPHYSICAL EXAMINATION AND TEMPERATURE CONTROL. Sci Heat Thermophys Stud 2005:378–411. https://doi.org/10.1016/B978-044451954-2/50013-8.

[88] Gao X, Zhou Z, Wang J, Tian H, Qing M, Jiang L, et al. Comparative study of the catalytic co-pyrolysis of microalgae (Chlorella Vulgaris) and polypropylene with acid and base catalysts toward valuable chemicals production. Fuel Process Technol 2023;241:107520. https://doi.org/10.1016/J.FUPROC.2022.107520.

[89] Weng J, Cheng Z, Zhang Y, Jiang C, Long L, Wang J, et al. Online evaluation of catalytic co-pyrolysis of hemicellulose and polypropylene over CaO catalyst. Fuel 2023;332:125993. https://doi.org/10.1016/J.FUEL.2022.125993.

[90] Ansari KB, Hassan SZ, Bhoi R, Ahmad E. Co-pyrolysis of biomass and plastic wastes: A review on reactants synergy, catalyst impact, process parameter, hydrocarbon fuel potential, COVID-19. J Environ Chem Eng 2021;9:106436. https://doi.org/10.1016/J.JECE.2021.106436.

[91] Ali L, Kuttiyathil MS, Altarawneh M. Catalytic upgrading of the polymeric constituents in Covid-19 masks. J Environ Chem Eng 2022;10:106978. https://doi.org/10.1016/J.JECE.2021.106978.

[92] Geschwindner C, Goedderz D, Li T, Bender J, Böhm B, Dreizler A. The effects of various flame retardants on the combustion of polypropylene: Combining optical diagnostics and pyrolysis fragment analysis. Polym Degrad Stab 2023;211:110321. https://doi.org/10.1016/J.POLYMDEGRADSTAB.2023.110321.

[93] Fina A, Tabuani D, Peijs T, Camino G. POSS grafting on PPgMA by one-step reactive blending. Polymer (Guildf) 2009;50:218–26. https://doi.org/10.1016/J.POLYMER.2008.11.002.

[94] Yang J, Yu Y, Li Y, Zhang Q, Zheng L, Luo T, et al. Inerting effects of ammonium polyphosphate on explosion characteristics of polypropylene dust. Process Saf Environ Prot 2019;130:221–30. https://doi.org/10.1016/J.PSEP.2019.08.015.

[95] Dittrich B, Wartig KA, Hofmann D, Mülhaupt R, Schartel B. Carbon black, multiwall carbon nanotubes, expanded graphite and functionalized graphene flame retarded polypropylene nanocomposites. Polym Adv Technol 2013;24:916–26. https://doi.org/10.1002/PAT.3165.

[96] Zoromba MS, Nour MA, Eltamimy HE, Abd El-Maksoud SA. Effect of modified layered double hydroxide on the flammability and mechanical properties of polypropylene. Sci Eng Compos Mater 2018;25:101–8. https://doi.org/10.1515/SECM-2016-0050.

[97] Hapuarachchi TD, Peijs T, Bilotti E. Thermal degradation and flammability behavior of polypropylene/clay/carbon nanotube composite systems. Polym Adv Technol 2013;24:331–8. https://doi.org/10.1002/PAT.3087.

[98] Lecouvet B, Sclavons M, Bourbigot S, Devaux J, Bailly C. Water-assisted extrusion as a novel processing route to prepare polypropylene/halloysite nanotube nanocomposites: Structure and properties. Polymer (Guildf) 2011;52:4284–95. https://doi.org/10.1016/J.POLYMER.2011.07.021.

[99] Ardila-Suárez C, Pablo Villegas J, Lins de Barros Neto E, Ghislain T, Lavoie JM. Waste surgical masks to fuels via thermochemical co-processing with waste motor oil and biomass. Bioresour Technol 2022;348:126798. https://doi.org/10.1016/J.BIORTECH.2022.126798.

[100] Skrzyniarz M, Sajdak M, Zajemska M, Iwaszko J, Biniek-Poskart A, Skibí Nski A, et al. Plastic Waste Management towards Energy Recovery during

the COVID-19 Pandemic: The Example of Protective Face Mask Pyrolysis 2022. https://doi.org/10.3390/en15072629.

[101] Wu X, Wu Y, Wu K, Chen Y, Hu H, Yang M. Study on pyrolytic kinetics and behavior: The co-pyrolysis of microalgae and polypropylene. Bioresour Technol 2015;192:522–8. https://doi.org/10.1016/J.BIORTECH.2015.06.029.

[102] Jeske H, Schirp A, Cornelius F. Development of a thermogravimetric analysis (TGA) method for quantitative analysis of wood flour and polypropylene in wood plastic composites (WPC). Thermochim Acta 2012;543:165–71. https://doi.org/10.1016/J.TCA.2012.05.016.

[103] Salema AA, Zaifullizan YM, Wong WH. Pyrolysis and combustion kinetics of disposable surgical face mask produced during Covid-19 pandemic. Https://DoiOrg/101080/1556703620222048140 2022;44:566–76. https://doi.org/10.1080/15567036.2022.2048140.

[104] Yousef S, Eimontas J, Striūgas N, Abdelnaby MA. A new strategy for butanol extraction from COVID-19 mask using catalytic pyrolysis process over ZSM-5 zeolite catalyst and its kinetic behavior. Thermochim Acta 2022;711:179198. https://doi.org/10.1016/J.TCA.2022.179198.

[105] Xu C, Cao L, Chen Y. Ternary blends based on poly (ethylene-naphthalate)/glass fibers/nitrile rubber: Preparation, properties and effect of dynamic vulcanization. Polym Test 2013;32:1529–37. https://doi.org/10.1016/J.POLYMERTESTING.2013.10.003.

[106] Yang S, Wu W, Jiao Y, Cai Z, Fan H. Preparation of NBR/Tannic acid composites by assembling a weak IPN structure. Compos Sci Technol 2017;153:40–7. https://doi.org/10.1016/J.COMPSCITECH.2017.10.002.

[107] Brum Dutra da Rocha E, de Sousa AMF, Furtado CRG. Properties Investigation of novel nitrile rubber composites with rockwool fibers. Polym Test 2020;82:106291.

https://doi.org/10.1016/J.POLYMERTESTING.2019.106291.

[108] Zedler Ł, Przybysz M, Klein M, Saeb MR, Formela K. Processing, physico-mechanical and thermal properties of reclaimed GTR and NBR/reclaimed GTR blends as function of various additives. Polym Degrad Stab 2017;143:186–95. https://doi.org/10.1016/J.POLYMDEGRADSTAB.2017.07.004.

[109] Pappa A, Mikedi K, Agapiou A, Karma S, Pallis GC, Statheropoulos M, et al. TG–MS analysis of nitrile butadiene rubber blends (NBR/PVC). J Anal Appl Pyrolysis 2011;92:106–10. https://doi.org/10.1016/J.JAAP.2011.05.003.

[110] Januszewicz K, Kazimierski P, Suchocki T, Kardaś D, Lewandowski W, Klugmann-Radziemska E, et al. Waste Rubber Pyrolysis: Product Yields and Limonene Concentration. Materials (Basel) 2020;13:1–14. https://doi.org/10.3390/MA13194435.

[111] Li MC, Zhang Y, Cho UR. Mechanical, thermal and friction properties of rice bran carbon/nitrile rubber composites: Influence of particle size and loading. Mater Des 2014;63:565–74. https://doi.org/10.1016/J.MATDES.2014.06.032.

[112] Iqbal N, Sagar S, Khan MB, Rafique HM. Ablation, thermal stability/transport and mechanical investigations of modified nanokaolinite impregnated acrylonitrile butadiene rubber composites n.d. https://doi.org/10.1177/0021998313484948.

[113] Nihmath A, Ramesan MT. Synthesis, characterization, processability, mechanical properties, flame retardant, and oil resistance of chlorinated acrylonitrile butadiene rubber. Polym Adv Technol 2018;29:2165–73. https://doi.org/10.1002/PAT.4324.

[114] Mensah B, Konadu DS, Nsaful F, Angnunavuri PN, Kwofie S. A systematic study of the effect of graphene oxide and reduced graphene oxide on the thermal degradation behavior of acrylonitrile-butadiene rubber in air and

nitrogen media. Sci African 2023;19:e01501. https://doi.org/10.1016/J.SCIAF.2022.E01501.

[115] Esmizadeh E, Chang BP, Jubinville D, Seto C, Ojogbo E, Tzoganakis C, et al. Stability of nitrile and vinyl latex gloves under repeated disinfection cycles. Mater Today Sustain 2021;11–12:100067. https://doi.org/10.1016/J.MTSUST.2021.100067.

[116] Su G, Ong HC, Ibrahim S, Fattah IMR, Mofijur M, Chong CT. Valorisation of medical waste through pyrolysis for a cleaner environment: Progress and challenges. Environ Pollut 2021;279:116934. https://doi.org/10.1016/J.ENVPOL.2021.116934.

[117] Özer B. A Study on coal combustion: experiments and modelling 2019.

[118] GÜREL K. SINGLE PARTICLE COMBUSTION ANALYSIS OF BIOMASS FUELS BY USING WIRE MESH REACTOR 2021.

[119] Akın SŞ. Investigation of fly ash characteristics on zeolite 4A synthesis 2019.

[120] Tomeczek J. Coal combustion 1992.

[121] Howard JB, Essenhigh RH. Pyrolysis of coal particles in pulverized fuel flames. Ind Eng Chem Process Des Dev 1967;6:74–84. https://doi.org/10.1021/I260021A013/ASSET/I260021A013.FP.PNG_V03.

[122] Sami M, Annamalai K, Wooldridge M. Co-firing of coal and biomass fuel blends. Prog Energy Combust Sci 2001;27:171–214. https://doi.org/10.1016/S0360-1285(00)00020-4.

[123] Zhang L, Xu S, Zhao W, Liu S. Co-pyrolysis of biomass and coal in a free fall reactor. Fuel 2007;86:353–9. https://doi.org/10.1016/J.FUEL.2006.07.004.

[124] Baghirzade M. Investigation of Turkish lignites and biomass at high heating rates by using wire mesh apparatus 2018.

[125] Ponte Jr GP da. Emergency control. Risk Manag Oil Gas Ind 2021:179–306.

https://doi.org/10.1016/B978-0-12-823533-1.00006-X.

[126] Wypych A, Wypych G. Information on data fields. Datab Green Solvents 2019:5–18. https://doi.org/10.1016/B978-1-927885-43-7.50004-4.

[127] Lu JJ, Chen WH. Investigation on the ignition and burnout temperatures of bamboo and sugarcane bagasse by thermogravimetric analysis. Appl Energy 2015;160:49–57. https://doi.org/10.1016/J.APENERGY.2015.09.026.

[128] Wen X, Szymańska K, Chen X, Mijowska E. Nanosized carbon black as synergist in PP/POE-MA/IFR system for simultaneously improving thermal, electrical and mechanical properties. J Therm Anal Calorim 2020;139:1091–8. https://doi.org/10.1007/S10973-019-08466-4/TABLES/5.

[129] Fina A, Cuttica F, Camino G. Ignition of polypropylene/montmorillonite nanocomposites. Polym Degrad Stab 2012;97:2619–26. https://doi.org/10.1016/J.POLYMDEGRADSTAB.2012.07.017.

[130] Liu Y, Gao Y, Zhang Z, Wang Q. Preparation of ammonium polyphosphate and dye co-intercalated LDH/polypropylene composites with enhanced flame retardant and UV resistance properties. Chemosphere 2021;277:130370. https://doi.org/10.1016/J.CHEMOSPHERE.2021.130370.

[131] Zhang S, Horrocks AR, Hull R, Kandola BK. Flammability, degradation and structural characterization of fibre-forming polypropylene containing nanoclay–flame retardant combinations. Polym Degrad Stab 2006;91:719–25. https://doi.org/10.1016/J.POLYMDEGRADSTAB.2005.05.023.

[132] Szefer EM, Majka TM, Pielichowski K. Characterization and Combustion Behavior of Single-Use Masks Used during COVID-19 Pandemic. Mater 2021, Vol 14, Page 3501 2021;14:3501. https://doi.org/10.3390/MA14133501.

[133] Gent S, Twedt M, Gerometta C, Almberg E. Torrefaction Bioenergy Generation. Theor Appl Asp Biomass Torrefaction 2017:123–50.

https://doi.org/10.1016/B978-0-12-809483-9.00006-3.

[134] Liu G, Xiao M, Zhang X, Gal C, Chen X, Liu L, et al. A review of air filtration technologies for sustainable and healthy building ventilation. Sustain Cities Soc 2017;32:375–96. https://doi.org/10.1016/j.scs.2017.04.011.

[135] Lv Y, Xu L, Niu Y, Wang G, Lei Y, Huang H, et al. Investigation on ash deposition formation during co-firing of coal with wheat straw. J Energy Inst 2022;100:148–59. https://doi.org/10.1016/J.JOEI.2021.11.009.

[136] Analysis of Ash Melting Behaviour (Oxidising Conditions) - Celignis Analytical n.d. https://www.celignis.com/package.php?value=40 (accessed August 28, 2023).

[137] Dalkhsuren D, Iwabuchi K, Itoh T, Narita T, Piash MI, Nachin B, et al. Effects of Ash Composition and Combustion Temperature on Reduced Particulate Matter Emission by Biomass Carbonization. Bioenergy Res 2022;16:1629–38. https://doi.org/10.1007/S12155-022-10526-X/TABLES/3.

[138] Youcai Z. Characterization and Recycling of Bottom Ash. Pollut Control Resour Recover Munic Solid Wastes Inciner 2017:61–82. https://doi.org/10.1016/B978-0-12-812165-8.00002-0.

[139] Puppala AJ, Pedarla A, Bheemasetti T. Soil Modification by Admixtures: Concepts and Field Applications. Gr Improv Case Hist Chem Electrokinet Therm Bioeng Methods 2015:291–309. https://doi.org/10.1016/B978-0-08-100191-2.00010-1.

[140] Cwirzen A. Properties of SCC with industrial by-products as aggregates. Self-Compacting Concr Mater Prop Appl 2020:249–81. https://doi.org/10.1016/B978-0-12-817369-5.00010-6.

[141] Alengaram UJ. Valorization of industrial byproducts and wastes as sustainable construction materials. Handb Sustain Concr Ind Waste Manag Recycl Artif Aggregate, Innov Eco-Friendly Bind Life Cycle Assess

2022:23–43. https://doi.org/10.1016/B978-0-12-821730-6.00003-6.

[142] Zhang B, Zhao Y, Zhao X, Huo Z. Study on Slagging Characteristics of Boiler Pre-combustion Chambers Based on Deep Learning. ACS Omega 2023;8:15620–30. https://doi.org/10.1021/ACSOMEGA.3C00998/ASSET/IMAGES/LARGE/AO3C00998_0013.JPEG.

[143] Sua-Iam G, Makul N. Utilization of coal- and biomass-fired ash in the production of self-consolidating concrete: a literature review. J Clean Prod 2015;100:59–76. https://doi.org/10.1016/J.JCLEPRO.2015.03.038.

[144] Colonna P, Berloco N, Ranieri V, Shuler ST. Application of Bottom Ash for Pavement Binder Course. Procedia - Soc Behav Sci 2012;53:961–71. https://doi.org/10.1016/J.SBSPRO.2012.09.945.

[145] Zhao L, Zhang FS, Chen M, Liu Z, Wu DBJ. Typical pollutants in bottom ashes from a typical medical waste incinerator. J Hazard Mater 2010;173:181. https://doi.org/10.1016/J.JHAZMAT.2009.08.066.

[146] Kim SY, Matsuto T, Tanaka N. Evaluation of pre-treatment methods for landfill disposal of residues from municipal solid waste incineration. Waste Manag Res 2003;21:416–23. https://doi.org/10.1177/0734242X0302100504.

[147] Miao J, Li J, Wang F, Xia X, Deng S, Zhang S. Characterization and evaluation of the leachability of bottom ash from a mobile emergency incinerator of COVID-19 medical waste: A case study in Huoshenshan Hospital, Wuhan, China. J Environ Manage 2022;303:114161. https://doi.org/10.1016/J.JENVMAN.2021.114161.

[148] Ibáñez R, Andrés A, Viguri JR, Ortiz I, Irabien JA. Characterisation and management of incinerator wastes. J Hazard Mater 2000;79:215–27. https://doi.org/10.1016/S0304-3894(00)00268-5.

[149] Farrokhi FY, Kazanç F. Combustion Behavior and Kinetics of Turkish Lignite

Blended with Biomass/Magnesite Dust. J Energy Eng 2018;144:04018064. https://doi.org/10.1061/(ASCE)EY.1943-7897.0000579.

[150] Magalhães D, Panahi A, Kazanç F, Levendis YA. Comparison of single particle combustion behaviours of raw and torrefied biomass with Turkish lignites. Fuel 2019;241:1085–94. https://doi.org/10.1016/J.FUEL.2018.12.124.

[151] TruSpec Micro | LECO Analytical Instruments n.d. https://www.leco.com/product/truspec-micro (accessed May 23, 2023).

[152] Akgül A, Palmeiro-Sanchez T, Lange H, Magalhaes D, Moore S, Paiva A, et al. Characterization of tars from recycling of PHA bioplastic and synthetic plastics using fast pyrolysis. J Hazard Mater 2022;439:129696. https://doi.org/10.1016/J.JHAZMAT.2022.129696.

[153] Magalhães D, Gürel K, Matsakas L, Christakopoulos P, Pisano I, Leahy JJ, et al. Prediction of yields and composition of char from fast pyrolysis of commercial lignocellulosic materials, organosolv fractionated and torrefied olive stones. Fuel 2021;289:119862. https://doi.org/10.1016/J.FUEL.2020.119862.

[154] Daéid NN. FORENSIC SCIENCES | Systematic Drug Identification. Encycl Anal Sci Second Ed 2005:471–80. https://doi.org/10.1016/B0-12-369397-7/00197-7.

[155] Trubetskaya A, Larsen FH, Shchukarev A, Ståhl K, Umeki K. Potassium and soot interaction in fast biomass pyrolysis at high temperatures. Fuel 2018;225:89–94. https://doi.org/10.1016/J.FUEL.2018.03.140.

[156] Trubetskaya A, Budarin V, Arshadi M, Magalhães D, Kazanç F, Hunt AJ. Supercritical extraction of biomass as an effective pretreatment step for the char yield control in pyrolysis. Renew Energy 2021;170:107–17. https://doi.org/10.1016/J.RENENE.2021.01.116.

[157] Kwapinska M, Pisano I, Leahy JJ. Preliminary Assessment of Pyrolysis Biochar Derived from Milk/Dairy Processing Sludge as a Potential Component of Fertilizers. ACS Sustain Chem Eng 2023;11:2345–53. https://doi.org/10.1021/ACSSUSCHEMENG.2C06093/ASSET/IMAGES/LARGE/SC2C06093_0002.JPEG.

[158] Christy Vijay JJ, Lawrence A, Arthanareeswaran G. Analytical Tool for Analysing Slagging Characteristic of High Ash Coals in Utility Boilers 2017.

[159] Lachman J, Baláš M, Lisý M, Lisá H, Milčák P, Elbl P. An overview of slagging and fouling indicators and their applicability to biomass fuels. Fuel Process Technol 2021;217:106804. https://doi.org/10.1016/J.FUPROC.2021.106804.

[160] Garcia-Maraver A, Mata-Sanchez J, Carpio M, Perez-Jimenez JA. Critical review of predictive coefficients for biomass ash deposition tendency. J Energy Inst 2017;90:214–28. https://doi.org/10.1016/J.JOEI.2016.02.002.

[161] Karthikeyan P, Subagunasekar M, Lenin N, Prabhu K. Abundance, spatial distribution, and chemical characterization of face masks on the beaches of SE Kanyakumari, India. Mar Pollut Bull 2023;192:115031. https://doi.org/10.1016/J.MARPOLBUL.2023.115031.

[162] Jung MR, Horgen FD, Orski S V., Rodriguez C. V, Beers KL, Balazs GH, et al. Validation of ATR FT-IR to identify polymers of plastic marine debris, including those ingested by marine organisms. Mar Pollut Bull 2018;127:704–16. https://doi.org/10.1016/J.MARPOLBUL.2017.12.061.

[163] De-la-Torre GE, Dioses-Salinas DC, Pizarro-Ortega CI, Fernández Severini MD, Forero López AD, Mansilla R, et al. Binational survey of personal protective equipment (PPE) pollution driven by the COVID-19 pandemic in coastal environments: Abundance, distribution, and analytical characterization. J Hazard Mater 2022;426:128070. https://doi.org/10.1016/J.JHAZMAT.2021.128070.

[164] Alhareb AO, Akil HBM, Ahmad ZAB. Poly(methyl methacrylate) denture base composites enhancement by various combinations of nitrile butadiene rubber/treated ceramic fillers. J Thermoplast Compos Mater 2017;30:1069–90. https://doi.org/10.1177/0892705715616856.

[165] Zhao L, Zhang FS, Wang K, Zhu J. Chemical properties of heavy metals in typical hospital waste incinerator ashes in China. Waste Manag 2009;29:1114–21. https://doi.org/10.1016/J.WASMAN.2008.09.003.

[166] Bakkali MEL, Bahri M, Gmouh S, Jaddi H, Bakkali M, Laglaoui A, et al. Characterization of bottom ash from two hospital waste incinerators in Rabat, Morocco. Waste Manag Res 2013;31:1228–36. https://doi.org/10.1177/0734242X13507308.

[167] Einhäuser TJ. ICP-OES and SEM-EDX Analysis of Dust and Powder Produced by the Laser-Processing of a Cr-Ni-Steel Alloy. Mikrochim Acta 1997;127:265–8. https://doi.org/10.1007/bf01242733.

[168] Trubetskaya A, Grams J, Leahy JJ, Johnson R, Gallagher P, Monaghan RFD, et al. The effect of particle size, temperature and residence time on the yields and reactivity of olive stones from torrefaction. Renew Energy 2020;160:998–1011. https://doi.org/10.1016/J.RENENE.2020.06.136.

[169] Quevauviller P, Imbert JL, Ollé M. Evaluation of the use of microwave oven systems for the digestion of environmental samples. Mikrochim Acta 1993;112:147–54. https://doi.org/10.1007/BF01243331/METRICS.

[170] Thurnau RC, Fournier D. The Behavior of Arsenic in a Rotary Kiln Incinerator. Http://DxDoiOrg/101080/10473289199210466982 2012;42:179–84. https://doi.org/10.1080/10473289.1992.10466982.

[171] Barton RG, Clark WD, Seeker WR. Fate of Metals in Waste Combustion Systems. Http://DxDoiOrg/101080/00102209008951696 2007;74:327–42. https://doi.org/10.1080/00102209008951696.

[172] Le Forestier L, Libourel G. Characterization of flue gas residues from municipal solid waste combustors. Environ Sci Technol 1998;32:2250–6. https://doi.org/10.1021/ES980100T/ASSET/IMAGES/LARGE/ES980100TF00003.JPEG.

[173] Zhang YL, Kasai E. Effect of chlorine on the vaporization behavior of zinc and lead during high temperature treatment of dust and fly ash. ISIJ Int 2004;44:1457–68. https://doi.org/10.2355/ISIJINTERNATIONAL.44.1457.

[174] Protocol on Heavy Metals | UNECE n.d. https://unece.org/environment-policy/air/protocol-heavy-metals (accessed February 20, 2023).

APPENDICES

A. Duplicate Results of Personal Protective Equipment Proximate Analysis

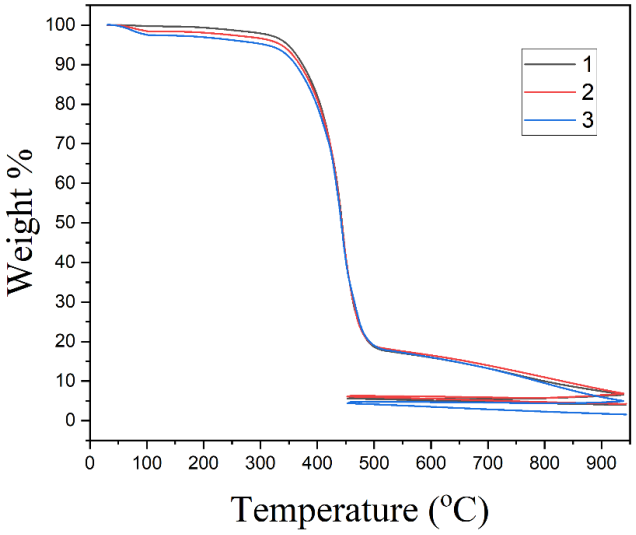

Figure A. 1 Duplicate TGA profiles of the nitrile glove

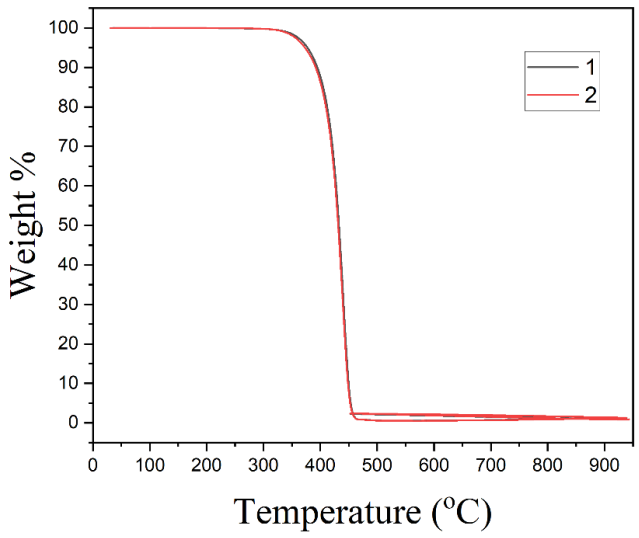

Figure A. 2 Duplicate TGA profiles of the medical gown

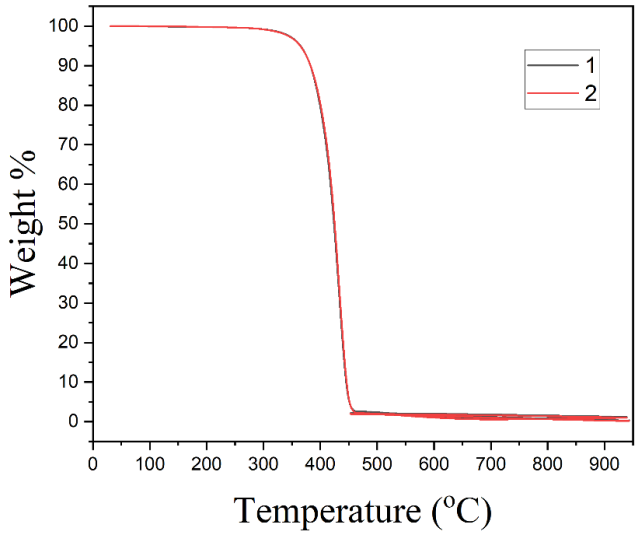

Figure A. 3 Duplicate TGA profiles of the face mask

B. Duplicate Results of Personal Protective Equipment Pyrolysis DTG Profiles

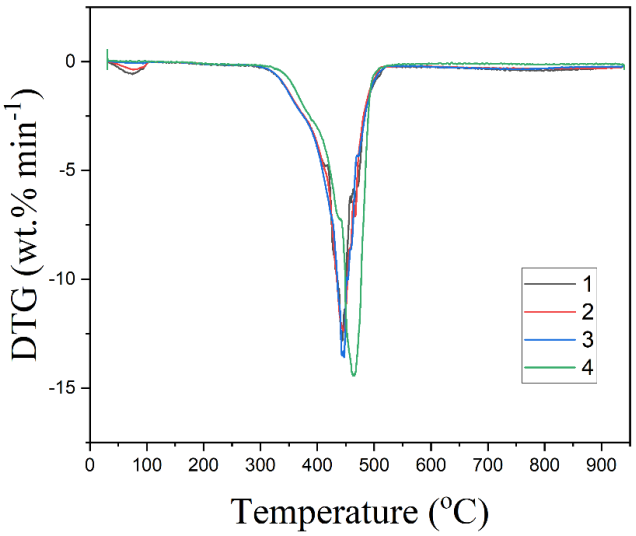

Figure B. 1 Duplicate pyrolysis DTG profiles of the nitrile glove

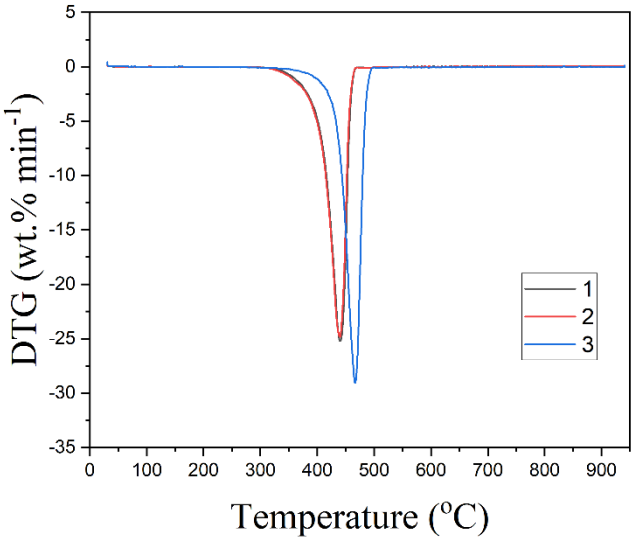

Figure B. 2 Duplicate pyrolysis DTG profiles of the medical gown

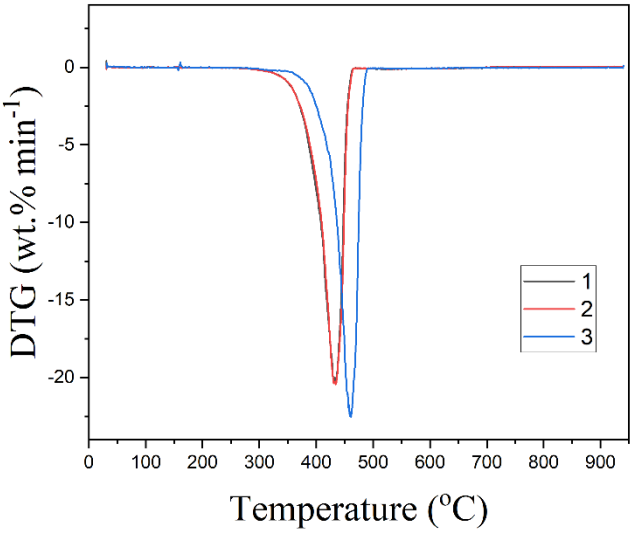

Figure B. 3 Duplicate pyrolysis DTG profiles of the face mask

C. Duplicate Results of Personal Protective Equipment Combustion DTG Profiles

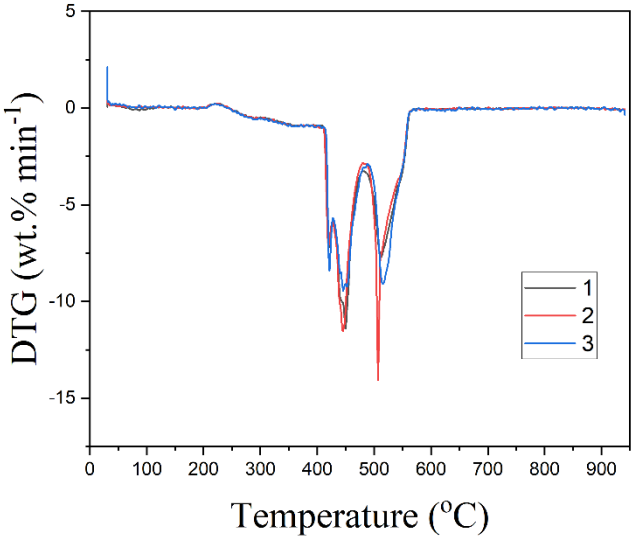

Figure C. 1 Duplicate combustion DTG profiles of the nitrile glove

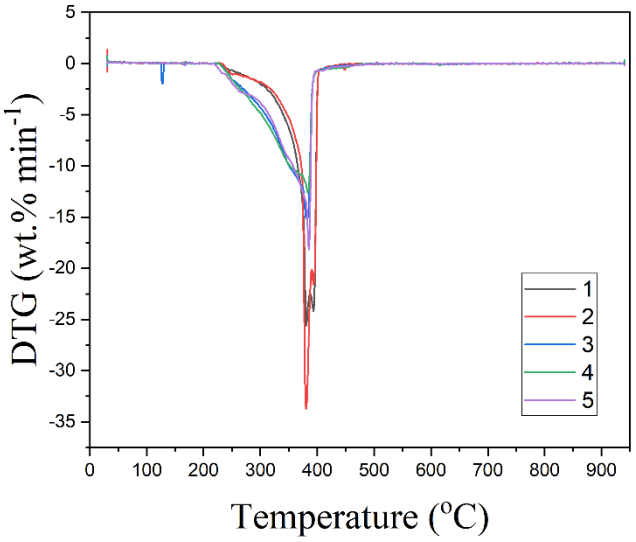

Figure C. 2 Duplicate combustion DTG profiles of the medical gown

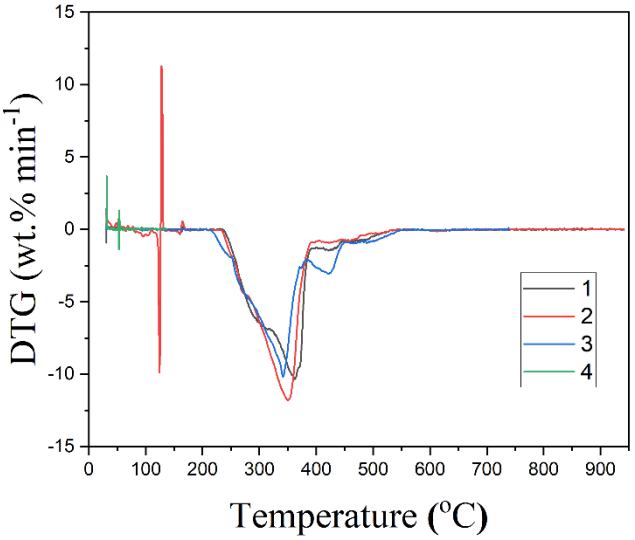

Figure C. 3 Duplicate combustion DTG profiles of the face mask

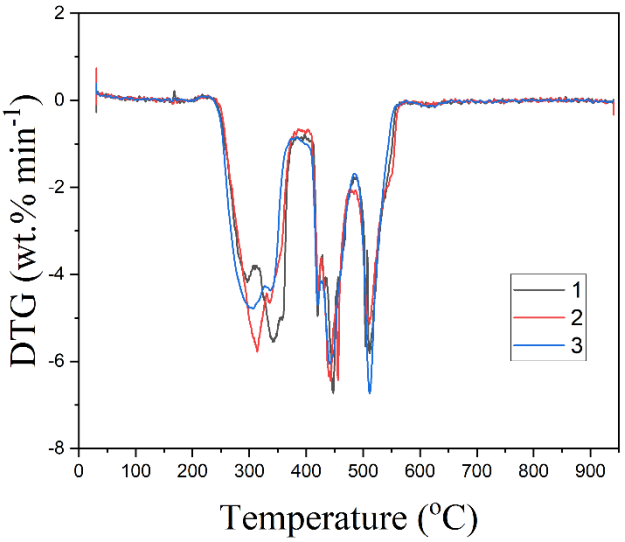

Figure C. 4 Duplicate combustion DTG profiles of GL60G20M20

D. Duplicate Results of Personal Protective Equipment in DSC

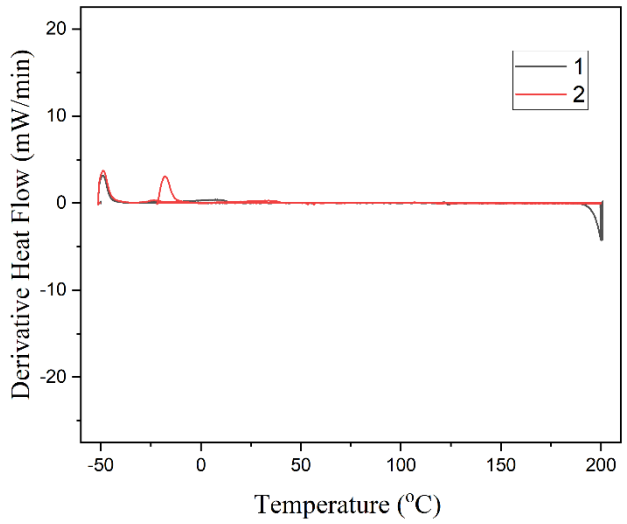

Figure D. 1 Duplicate DSC profile of nitrile glove

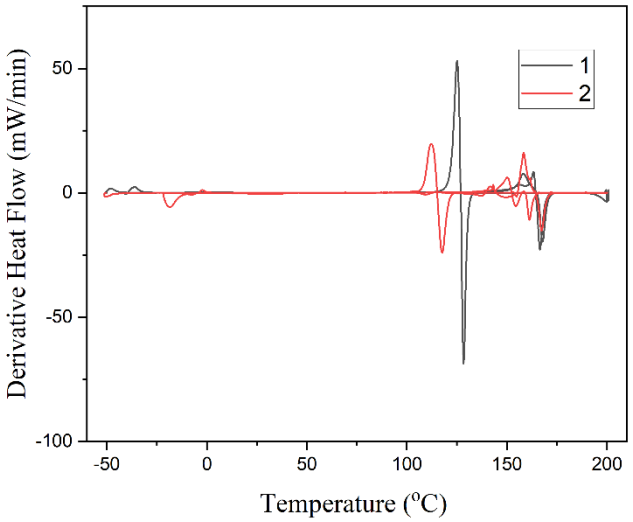

Figure D. 2 Duplicate DSC profile of medical gown

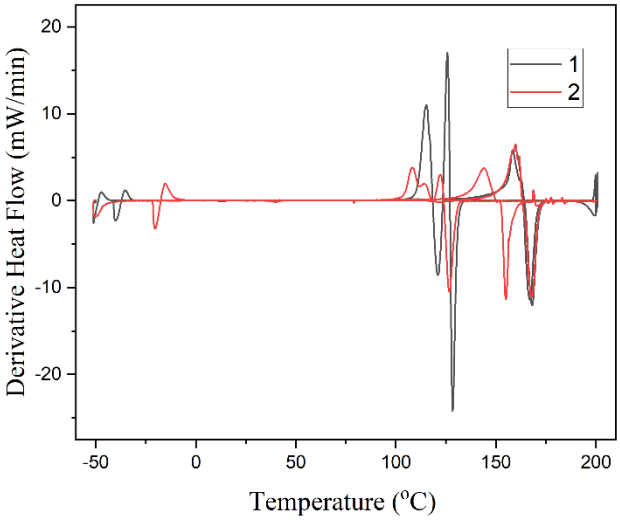

Figure D. 3 Duplicate DSC profile of face mask

E. Duplicate Results of Personal Protective Equipment Elemental Analysis

For EDX analysis, data was gathered from at least three randomly selected points. The average data was used in the results section, and the specific measurements were provided in the tables below.

Table E. 1 Nitrile glove combustion bottom ash elemental analysis results obtained with SEM-EDX

	Nitrile Glove		
	1	2	3
O	43.83	48.11	42.88
Al	1.88	1.48	1.1
S	9.11	8.67	9.71
Ca	11.75	11.75	13.11
Ti	20.72	20.29	21.37
Zn	12.71	9.71	11.83

Table E. 2 Medical gown combustion bottom ash elemental analysis results obtained with SEM-EDX

	Medical Gown			
	1	2	3	4
C	8.64	0.00	8.45	29.38
O	37.10	35.34	36.97	29.18
Al	3.40	3.72	3.81	2.16
Si	1.97	2.35	3.29	1.62
Ca	5.42	5.59	4.88	4.40
Ti	35.43	42.19	35.64	26.67
Cu	8.04	10.82	6.96	5.64
S	0.00	0.00	0.00	0.96

Table E. 3 Face mask combustion bottom ash elemental analysis results obtained with SEM-EDX

	Face Mask			
	1	2	3	4
C	13.37	11.19	23.94	7.74
O	39.96	23.79	28.50	42.09
Mg	3.91	2.23	2.57	2.22
Al	2.40	2.40	1.88	1.97
Ca	8.86	19.40	11.75	12.55
Ti	31.49	40.98	30.25	32.68
Si	0.00	0.00	1.12	0.75

Table E. 4 GL60G20M20 combustion bottom ash elemental analysis results obtained with SEM-EDX

	GL60G20M20			
	1	2	3	4
C	35.83	26.84	34.13	22.50
O	26.45	17.30	31.27	37.06
Na	4.30	3.45	6.86	7.07
Al	0.64	1.00	0.83	0.80
S	4.75	6.15	4.35	7.79
Ca	7.16	11.51	5.57	7.56
Ti	13.18	21.46	10.34	10.26
Zn	7.03	11.63	6.24	5.38
K	0.00	0.65	0.40	1.58
Ta	0.66	0.00	0.00	0.00